

# Angular analysis of $B_s \rightarrow f'_2(1525) (\rightarrow K^+ K^-) \mu^+ \mu^-$ decays as a probe to lepton flavor universality violation

N Rajeev<sup>1,\*</sup>, Niladribihari Sahoo<sup>2,†</sup> and Rupak Dutta<sup>1‡</sup>

<sup>1</sup>*National Institute of Technology Silchar, Silchar 788010, India*

<sup>2</sup>*Department of Physics, University of Warwick, Coventry CV4 7AL, United Kingdom*

The flavor anomalies reported in  $R_K$ ,  $R_{K^*}$ ,  $P'_5$  and  $\mathcal{B}(B_s \rightarrow \phi \mu^+ \mu^-)$  indicate lepton flavor universality violation in  $b \rightarrow s l^+ l^-$  quark level transition decays. The deviation from the SM prediction reported in the underlying flavor observables currently stand at the level of  $2.5\sigma$ ,  $2.4\sigma$ ,  $3.3\sigma$  and  $3.7\sigma$ , respectively. In this context, we perform an angular analysis of the four-body differential decay of  $B_s \rightarrow f'_2(1525) (\rightarrow K^+ K^-) \mu^+ \mu^-$  in a model independent effective field theory framework. The decay mode  $B_s \rightarrow f'_2(1525) l^+ l^-$  undergoes similar  $b \rightarrow s$  neutral current quark level transition and, in principle, can provide complementary information regarding lepton flavor universality violation in  $b \rightarrow s l^+ l^-$  quark level transition decays. We give predictions of various physical observables such as the branching ratio, the longitudinal polarization fraction, the forward-backward asymmetry, the angular observables  $P_1$ ,  $P_2$ ,  $P'_4$ ,  $P'_5$  and also the lepton flavor sensitive observables such as the ratio of branching ratio  $R_{f'_2}$ ,  $Q_{FL}$ ,  $Q_{AFB}$ ,  $Q_1$ ,  $Q_2$ ,  $Q'_4$ ,  $Q'_5$  for  $B_s \rightarrow f'_2(1525) (\rightarrow K^+ K^-) \mu^+ \mu^-$  decays in the standard model and in the presence of several 1D and 2D new physics scenarios.

## I. INTRODUCTION

Exploring and identifying the Lorentz structure of possible new physics (NP) that lies beyond the standard model (SM) is of great importance particularly in semileptonic  $B$  meson decays mediated via  $b \rightarrow s l^+ l^-$  neutral current and  $b \rightarrow c l \nu$  charged current interactions. It is well known that the flavor sector could be an ideal platform to explore NP since it can provide possible indirect evidence of NP in the form of new interactions that can, in principle, be very sensitive to the existing experiments. It is also well known that, apart from the flavor sector, existence of NP is also evident from several other phenomena such as the matter antimatter asymmetry of the universe, neutrino mass, dark matter, dark energy and so on. In the recent years, several measurements have shown hints of lepton flavor universality violation (LFUV) in the semileptonic decays of  $B$  mesons involving  $b \rightarrow s l^+ l^-$  ( $l \in e, \mu$ ) neutral current and  $b \rightarrow c l \nu$  ( $l \in e/\mu, \tau$ ) charged current quark level transitions. Significant deviation from the SM expectation has been reported in various flavor observables such as  $R_K$ ,  $R_{K^*}$ ,  $P'_5$  in  $B \rightarrow K^{(*)} l^+ l^-$  decays;  $\mathcal{B}(B_s \rightarrow \phi \mu^+ \mu^-)$ ;  $R_D$ ,  $R_{D^*}$ ,  $P_{D^*}^T$ ,  $F_L^{D^*}$  in  $B \rightarrow D^{(*)} l \nu$  decays and  $R_{J/\Psi}$  in  $B_c \rightarrow J/\Psi l \nu$  decays. Here we will focus mainly on the anomalies present in  $B$  meson decays mediated via  $b \rightarrow s l^+ l^-$  quark level transitions. The ratio of branching ratio  $R_K$  and  $R_{K^*}$  in  $B \rightarrow (K, K^*) l^+ l^-$  decays are defined as

$$R_{K^{(*)}} = \frac{\mathcal{B}(B \rightarrow K^{(*)} \mu^+ \mu^-)}{\mathcal{B}(B \rightarrow K^{(*)} e^+ e^-)}. \quad (1)$$

After the Rencontres de Moriond, 2019, the current status of several observables pertaining to  $b \rightarrow s l^+ l^-$  quark level transition decays is as follows: the measurement of  $R_K$  from the combined data of both Run 1 and Run 2 of LHCb reports  $R_K = 0.846_{-0.054}^{+0.060}$  (stat)  $_{-0.014}^{+0.016}$  (syst) [1] in the central  $q^2$  region ( $1 \leq q^2 \leq 6 \text{ GeV}^2$ ) where,  $q^2$  is the invariant mass-squared of the dilepton. The deviation from the SM value of  $R_K \sim 1$  [2, 3] is found to be at the level of  $\sim 2.5\sigma$ . Similarly, the  $R_{K^*}$  was measured in two different  $q^2$  bins from two different experiments where, the LHCb reports  $R_{K^*} = 0.660_{-0.070}^{+0.110}$  (stat)  $\pm 0.024$  (syst) [4] and Belle reports  $R_{K^*} = 0.52_{-0.26}^{+0.36}$  (stat)  $\pm 0.05$  (syst) [5] in the low  $q^2$  bin ( $0.045 \leq q^2 \leq 1.1 \text{ GeV}^2$ ) and similarly in the central  $q^2$  bin ( $1.1 \leq q^2 \leq 6 \text{ GeV}^2$ ), LHCb reports  $R_{K^*} = 0.685_{-0.069}^{+0.113}$  (stat)  $\pm 0.047$  (syst) [4] and Belle reports  $R_{K^*} = 0.96_{-0.29}^{+0.45}$  (stat)  $\pm 0.11$  (syst) [5]. These measurements differ from

\*Electronic address: rajeev\_rs@phy.nits.ac.in

†Electronic address: niladri.sahoo@warwick.ac.uk

‡Electronic address: rupak@phy.nits.ac.in

the SM prediction of  $R_{K^*} \sim 1$  [2, 3] at the level of  $\sim 2.4\sigma$ . In addition to  $R_K$  and  $R_{K^*}$ , the deviation from the SM expectation is also found in the measurements of the angular distributions of  $B \rightarrow K^* \mu^+ \mu^-$ , particularly in  $P'_5$  [6, 7]. The ATLAS [8] and LHCb [9, 10] collaborations measured  $P'_5$  in the bin  $q^2 \in [4, 6]$  GeV<sup>2</sup> and they differ by  $\sim 3.3\sigma$  [11] from the SM expectation [7]. Similarly, the CMS [12] measurement in  $q^2 \in [4.3, 6]$  GeV<sup>2</sup> and the Belle [13] measurement in  $q^2 \in [4.3, 8]$  GeV<sup>2</sup> differ by  $1\sigma$  and  $2.1\sigma$ , respectively from the SM expectations [6, 14]. In addition, the measured value of the branching ratio  $\mathcal{B}(B_s \rightarrow \phi \mu^+ \mu^-)$  [15, 16] is found to deviate at the level of  $\sim 3.7\sigma$  from the SM expectations [11, 17]. In Table I we report the current status of  $R_K$ ,  $R_{K^*}$  and  $P'_5$ . At present, the dedicated ongoing  $B$  factory programs at Belle II and LHCb emerge as promising platforms that can either confirm or refute the existence of NP in  $b \rightarrow s l^+ l^-$  transition decays.

	$q^2$ bins	Theoretical predictions	Experimental measurements	Deviation
$R_K$	[1.0, 6.0]	$1 \pm 0.01$ [2, 3]	$0.846^{+0.060}_{-0.054}$ (stat) $^{+0.016}_{-0.014}$ (syst) [1]	$\sim 2.5\sigma$
$R_{K^*}$	[0.045, 1.1]	$1 \pm 0.01$ [2, 3]	$0.660^{+0.110}_{-0.070}$ (stat) $\pm 0.024$ (syst) [4]	$\sim 2.4\sigma$
		$1 \pm 0.01$ [2, 3]	$0.52^{+0.36}_{-0.26}$ (stat) $\pm 0.05$ (syst) [5]	
	[1.1, 6.0]	$1 \pm 0.01$ [2, 3]	$0.685^{+0.113}_{-0.069}$ (stat) $\pm 0.047$ (syst) [4]	
		$1 \pm 0.01$ [2, 3]	$0.96^{+0.45}_{-0.29}$ (stat) $\pm 0.11$ (syst) [5]	
$P'_5$	[4.0, 6.0]	$-0.757 \pm 0.074$ [7]	$-0.21 \pm 0.15$ [8–10]	$\sim 3.3\sigma$
	[4.3, 6.0]	$-0.774^{+0.061+0.087}_{-0.059-0.093}$ [6]	$-0.96^{+0.22}_{-0.21}$ (stat) $\pm 0.16$ (syst) [12]	$\sim 1.0\sigma$
	[4.0, 8.0]	$-0.881 \pm 0.082$ [14]	$-0.267^{+0.275}_{-0.269}$ (stat) $\pm 0.049$ (syst) [13]	$\sim 2.1\sigma$

TABLE I: Current status of  $R_K$  and  $R_{K^*}$  and  $P'_5$  in  $B \rightarrow K^{(*)} l^+ l^-$  decays

Our main aim is to study the impact of NP on  $B_s \rightarrow f'_2(1525) \mu^+ \mu^-$  decay observables in a model independent effective theory formalism. The  $B_s \rightarrow f'_2(1525) \mu^+ \mu^-$  decay mode has received less attention both from the theoretical and the experimental side and it has not been discussed earlier in detail. Although, in Ref. [18], the authors discussed the SM results for both the  $\mu$  mode and  $\tau$  mode of  $B_s \rightarrow f'_2(1525) l^+ l^-$  along with the  $B \rightarrow K_2^*(1430) l^+ l^-$  decays, but more emphasis was given to  $B \rightarrow K_2^*$  rather than  $B_s \rightarrow f'_2$  decays. Also the branching ratio of  $f'_2$  decaying into  $K^+ K^-$  was not considered in their numerical analysis. In Ref. [18], the authors also discussed the impact of NP on several observables coming from two different NP models such as the vector-like quark model and the family non-universal  $Z'$  model. Similarly, there are ample number of literatures discussing the  $B \rightarrow K_2^*(1430) l^+ l^-$  decays [19–26] mediated via same  $b \rightarrow s l^+ l^-$  quark level transition.

So far we don't have many experimental results on electroweak penguin decays involving spin 2 particles. The experimental techniques used for  $B_s \rightarrow \phi l^+ l^-$  can be adjusted to  $B_s \rightarrow f'_2(1525) l^+ l^-$  decay as well because both  $\phi$  and  $f'_2(1525)$  decay to a pair of charged kaons which are easily detected by the LHCb detector. Since the dominating structures in  $K^+ K^-$  spectrum are the P wave  $\phi(1020)$ , and there are several possible resonances around 1500 MeV/ $c^2$ , it's a natural thing to look at this regime to study. Further, the presence of D waves in this mass region yields a richer spectrum for exploring interesting angular observables. Moreover, we will show afterwards that the branching ratio of this decay mode is found to be sizable using pQCD form factors, hence we expect hundreds of signal events to be observed by analyzing the current LHCb data available.

The present paper is organized as follows: in Section II, we start with a brief overview of the effective Hamiltonian for  $b \rightarrow s l^+ l^-$  quark level transition decays in the presence of new vector and axial vector NP operators. A brief discussion of  $B_s \rightarrow f'_2$  hadronic matrix elements followed by the angular distribution and the transversity amplitudes for  $B_s \rightarrow f'_2(1525)(\rightarrow K^+ K^-) \mu^+ \mu^-$  decays are also reported. Finally we write down the decay distribution and expressions for several lepton flavor universal (LFU) observables. In Section III, we report our results that are obtained in the SM and in several NP scenarios. We conclude with a brief summary of our results in Section IV.

## II. THEORETICAL FRAMEWORK

### A. Effective Hamiltonian

The effective Hamiltonian for  $b \rightarrow s l^+ l^-$  quark level transition decays in the presence of new vector and axial vector NP operators is written as [27],

$$\mathcal{H}_{eff} = -\frac{G_F}{\sqrt{2}} V_{tb} V_{ts}^* \frac{\alpha_e}{4\pi} \left[ C_9^{eff} \bar{s} \gamma^\mu P_L b \bar{l} \gamma_\mu l + C_{10}^{eff} \bar{s} \gamma^\mu P_L b \bar{l} \gamma_\mu \gamma_5 l - \frac{2m_b}{q^2} C_7^{eff} \bar{s} i q_\nu \sigma^{\mu\nu} P_R b \bar{l} \gamma_\mu l + \right. \\ \left. C_9^{NP} \bar{s} \gamma^\mu P_L b \bar{l} \gamma_\mu l + C_{10}^{NP} \bar{s} \gamma^\mu P_L b \bar{l} \gamma_\mu \gamma_5 l + C'_9 \bar{s} \gamma^\mu P_R b \bar{l} \gamma_\mu l + C'_{10} \bar{s} \gamma^\mu P_R b \bar{l} \gamma_\mu \gamma_5 l \right], \quad (2)$$

where  $G_F$  is the Fermi coupling constant,  $\alpha_e$  is the fine structure constant,  $V_{tb}$  and  $V_{ts}$  are the corresponding Cabibbo Kobayashi Maskawa (CKM) matrix elements and  $P_{L,R} = (1 \mp \gamma_5)/2$ . The factorizable loop terms are incorporated within the effective Wilson coefficients (WCs)  $C_7^{eff}$  and  $C_9^{eff}$  as [28]

$$C_7^{eff} = C_7 - \frac{C_5}{3} - C_6 \\ C_9^{eff} = C_9(\mu) + h(\hat{m}_c, \hat{s}) C_0 - \frac{1}{2} h(1, \hat{s})(4C_3 + 4C_4 + 3C_5 + C_6) \\ - \frac{1}{2} h(0, \hat{s})(C_3 + 3C_4) + \frac{2}{9}(3C_3 + C_4 + 3C_5 + C_6), \quad (3)$$

where,  $\hat{s} = q^2/m_b^2$ ,  $\hat{m}_c = m_c/m_b$ , and  $C_0 = 3C_1 + C_2 + 3C_3 + C_4 + 3C_5 + C_6$ . Similarly, the auxiliary functions are defined as

$$h(z, \hat{s}) = -\frac{8}{9} \ln \frac{m_b}{\mu} - \frac{8}{9} \ln z + \frac{8}{27} + \frac{4}{9}x - \frac{2}{9}(2+x)|1-x|^{1/2} \begin{cases} \ln \left| \frac{\sqrt{1-x}+1}{\sqrt{1-x}-1} \right| - i\pi, & \text{for } x \equiv \frac{4z^2}{\hat{s}} < 1 \\ 2 \arctan \frac{1}{\sqrt{x-1}}, & \text{for } x \equiv \frac{4z^2}{\hat{s}} > 1 \end{cases} \quad (4)$$

$$h(0, \hat{s}) = -\frac{8}{9} \ln \frac{m_b}{\mu} - \frac{4}{9} \ln \hat{s} + \frac{8}{27} + \frac{4}{9}i\pi. \quad (5)$$

The additional terms in the  $C_9^{eff}$  describe the short distance contributions from the four-quark operators which lie away from the  $c\bar{c}$  resonance region. Similarly, the long distance contributions which include the resonant state from  $b \rightarrow c\bar{c}s$  which further annihilate into a lepton pair are excluded in the present analysis. Hence, we only concentrate on the regions from  $q^2 \in [0.045, 0.98]$  and  $q^2 \in [1.1, 6.0]^1$  GeV<sup>2</sup>. The new WCs in the effective Hamiltonian such as  $C_{9,10}^{NP}$  and  $C'_{9,10}$  include the effects coming from the new vector and axial vector NP couplings. In SM, all these new WCs are considered to be zero. In principle, one can have the new scalar, pseudoscalar and tensor NP WCs but they are severely constrained by  $B_s \rightarrow \mu^+ \mu^-$  and  $b \rightarrow s\gamma$  measurements [29–31]. The values for each WC obtained in the leading logarithmic approximation at the energy scale  $\mu = m_{b,pole}$  are reported in Table III. Similarly, the values of each new WCs are obtained from the global fits reported in the Ref. [32].

### B. Spin 2 polarization tensor and $B_s \rightarrow f'_2$ hadronic matrix elements

A spin 2 polarization tensor  $\epsilon^{\mu\nu}(n)$ , where  $(n \in \pm 2, \pm 1, 0)$ , can be constructed via spin 1 polarization vector [18, 33, 34]. For the  $f'_2$  meson having the four momentum  $(|\vec{p}_{f'_2}|, 0, 0, E_{f'_2})$ , where,  $\vec{p}_{f'_2}$  and  $E_{f'_2}$  are the momentum and energy of  $f'_2$  in the  $B_s$  meson rest frame, the explicit structure of polarization tensor  $\epsilon^{\mu\nu}(n)$  in the ordinary coordinate frame are constructed out of a massive vector state by the use of an appropriate Clebsch-Gordan coefficients. Those

<sup>1</sup> The  $q^2 \in [0.98, 1.1]$  GeV<sup>2</sup> is excluded because of  $\phi(1020) \rightarrow \mu^+ \mu^-$  decays.

are

$$\begin{aligned}
\epsilon_{\mu\nu}(\pm 2) &= \epsilon_\mu(\pm) \epsilon_\nu(\pm) \\
\epsilon_{\mu\nu}(\pm 1) &= \frac{1}{\sqrt{2}} \left[ \epsilon_\mu(\pm) \epsilon_\nu(0) + \epsilon_\nu(\pm) \epsilon_\mu(0) \right] \\
\epsilon_{\mu\nu}(0) &= \frac{1}{\sqrt{6}} \left[ \epsilon_\mu(+) \epsilon_\nu(-) + \epsilon_\nu(+) \epsilon_\mu(-) \right] + \sqrt{\frac{2}{3}} \epsilon_\mu(0) \epsilon_\nu(0),
\end{aligned} \tag{6}$$

where

$$\epsilon_\mu(0) = \frac{1}{m_{f'_2}} (|\vec{p}_{f'_2}|, 0, 0, E_{f'_2}), \quad \epsilon_\mu(\pm) = \frac{1}{\sqrt{2}} (0, \mp 1, -i, 0). \tag{7}$$

In the  $B_s \rightarrow f'_2(1525) l^+ l^-$  decay, the  $n = \pm 2$  helicity states of the  $f'_2$  are not aware of the two leptons that are obtained in the final state. Hence, it would be convenient to introduce a new polarization vector  $\epsilon_{T_\mu}(h)$  as

$$\epsilon_{T_\mu}(h) = \frac{1}{m_b} \epsilon_{\mu\nu}(h) P_{B_s}^\nu \tag{8}$$

where  $P_{B_s}$  is the four momentum of  $B_s$  meson. The polarization vector  $\epsilon_{T_\mu}(h)$  satisfies the following equations [18].

$$\begin{aligned}
\epsilon_{T_\mu}(\pm 2) &= 0, \\
\epsilon_{T_\mu}(\pm 1) &= \frac{1}{m_{B_s}} \frac{1}{\sqrt{2}} \epsilon(0) \cdot P_{B_s} \epsilon_\mu(\pm) = \frac{\sqrt{\lambda}}{\sqrt{8} m_{B_s} m_{f'_2}} \epsilon_\mu(\pm), \\
\epsilon_{T_\mu}(0) &= \frac{1}{m_{B_s}} \sqrt{\frac{2}{3}} \epsilon(0) \cdot P_{B_s} \epsilon_\mu(0) = \frac{\sqrt{\lambda}}{\sqrt{6} m_{B_s} m_{f'_2}} \epsilon_\mu(0)
\end{aligned} \tag{9}$$

In general, the  $B_s \rightarrow f'_2$  hadronic matrix elements can be parameterized in terms of several form factors as follows [18, 21, 22, 34, 35]:

$$\begin{aligned}
\langle f'_2(P_{f'_2}, \epsilon) | \bar{s} \gamma^\mu b | \bar{B}_s(P_{B_s}) \rangle &= -\frac{2V(q^2)}{m_{B_s} + m_{f'_2}} \epsilon^{\mu\nu\rho\sigma} \epsilon_{T_\nu}^* P_{B_s\rho} P_{f'_2\sigma} \\
\langle f'_2(P_{f'_2}, \epsilon) | \bar{s} \gamma^\mu \gamma_5 b | \bar{B}_s(P_{B_s}) \rangle &= 2i m_{f'_2} A_0(q^2) \frac{\epsilon_{T \cdot q}^*}{q^2} q^\mu + i(m_{B_s} + m_{f'_2}) A_1(q^2) \left[ \epsilon_{T_\mu}^* - \frac{\epsilon_{T \cdot q}^*}{q^2} q^\mu \right] \\
&\quad - i A_2(q^2) \frac{\epsilon_{T \cdot q}^*}{m_{B_s} + m_{f'_2}} \left[ P^\mu - \frac{m_{B_s}^2 + m_{f'_2}^2}{q^2} q^\mu \right] \\
\langle f'_2(P_{f'_2}, \epsilon) | \bar{s} \sigma^{\mu\nu} q_\nu b | \bar{B}_s(P_{B_s}) \rangle &= -2i T_1(q^2) \epsilon^{\mu\nu\rho\sigma} \epsilon_{T_\nu}^* P_{B_s\rho} P_{f'_2\sigma} \\
\langle f'_2(P_{f'_2}, \epsilon) | \bar{s} \sigma^{\mu\nu} \gamma_5 q_\nu b | \bar{B}_s(P_{B_s}) \rangle &= T_2(q^2) \left[ (m_{B_s}^2 + m_{f'_2}^2) \epsilon_{T_\mu} \epsilon_{T \cdot q}^* P^\mu \right] + T_3(q^2) \epsilon_{T \cdot q}^* \left[ q^\mu - \frac{q^2}{m_{B_s}^2 + m_{f'_2}^2} P^\mu \right], \tag{10}
\end{aligned}$$

where  $P_{B_s}$  and  $P_{f'_2}$  are the four momenta of  $B_s$  meson and  $f'_2$ , respectively and  $q = P_{B_s} - P_{f'_2}$ . In general, the  $B_s \rightarrow f'_2$  transition form factors are non-perturbative in nature and they can be calculated using several non-perturbative approaches. We follow Ref. [34] and write the  $B_s \rightarrow f'_2$  transition form factors as

$$F(q^2) = \frac{F(0)}{(1 - q^2/m_{B_s}^2) [1 - a(q^2/m_{B_s}^2) + b(q^2/m_{B_s}^2)]}, \tag{11}$$

where  $F$  denotes  $A_0$ ,  $A_1$ ,  $V$ ,  $T_1$ ,  $T_2$  and  $T_3$ , respectively. Similarly,  $A_2$  is related to  $A_0$  and  $A_1$  by

$$A_2(q^2) = \frac{m_{B_s} + m_{f'_2}}{m_{B_s}^2 - q^2} [(m_{B_s} + m_{f'_2}) A_1(q^2) - 2 m_{f'_2} A_0(q^2)] \tag{12}$$

The numerical entries of the  $B_s \rightarrow f'_2$  form factors at the maximum recoil point and the two fitted parameters  $a$  and  $b$  are reported in Table IV. We refer to Ref. [34] for all the omitted details.

### C. Angular distribution and the transversity amplitudes for $B_s \rightarrow f'_2(1525)(\rightarrow K^+ K^-) \mu^+ \mu^-$

The decay amplitude for  $B_s \rightarrow f'_2(1525) l^+ l^-$  can be obtained from the effective Hamiltonian of Eq 2. Using the helicity techniques of Ref [18], the differential decay width of the four-body decay of  $B_s \rightarrow f'_2(1525)(\rightarrow K^+ K^-) \mu^+ \mu^-$  can be written in terms of several angular coefficients as

$$\frac{d^4\Gamma}{dq^2 d\cos\theta_K d\cos\theta_l d\phi} = \frac{3}{8} \left[ I_1^c C^2 + 2 I_1^s S^2 + (I_2^c C^2 + 2 I_2^s S^2) \cos 2\theta_l + 2 I_3 S^2 \sin^2 \theta_l \cos 2\phi + \right. \\ \left. 2\sqrt{2} I_4 C S \sin 2\theta_l \cos \phi + 2\sqrt{2} I_5 C S \sin \theta_l \cos \phi + 2 I_6 S^2 \cos \theta_l + \right. \\ \left. 2\sqrt{2} I_7 C S \sin \theta_l \sin \phi + 2\sqrt{2} I_8 C S \sin 2\theta_l \sin \phi + 2 I_9 S^2 \sin^2 \theta_l \sin 2\phi \right], \quad (13)$$

where,  $C = C(f'_2) \equiv \sqrt{\frac{5}{16\pi}}(3 \cos^2 \theta_K - 1)$  and  $S = S(f'_2) \equiv \sqrt{\frac{15}{32\pi}} \sin(2\theta_K)$ . The direction of  $f'_2$  is chosen along the  $z$  direction in the  $B_s$  meson rest frame. The polar angle  $\theta_K$  ( $\theta_l$ ) is defined as the angle between the direction of  $K^-$  ( $\mu^-$ ) and the  $z$  axis in the rest frame of the lepton pair. Similarly,  $\phi$  is the angle between the decay planes of  $f'_2$  and the lepton pair. Moreover, the angular coefficients  $I_i(q^2)$  are defined as

$$\begin{aligned} I_1^c &= \left( |A_{L0}|^2 + |A_{R0}|^2 \right) + 8 \frac{m_l^2}{q^2} \text{Re} \left[ A_{L0} A_{R0}^* \right] + 4 \frac{m_l^2}{q^2} |A_t|^2, \\ I_2^c &= -\beta_l^2 \left( |A_{L0}|^2 + |A_{R0}|^2 \right), \\ I_1^s &= \frac{3}{4} \left[ |A_{L\perp}|^2 + |A_{L\parallel}|^2 + |A_{R\perp}|^2 + |A_{R\parallel}|^2 \right] \left( 1 - \frac{4m_l^2}{3q^2} \right) + \frac{4m_l^2}{q^2} \text{Re} \left[ A_{L\perp} A_{R\perp}^* + A_{L\parallel} A_{R\parallel}^* \right], \\ I_2^s &= \frac{1}{4} \beta_l^2 \left[ |A_{L\perp}|^2 + |A_{L\parallel}|^2 + |A_{R\perp}|^2 + |A_{R\parallel}|^2 \right], \\ I_3 &= \frac{1}{2} \beta_l^2 \left[ |A_{L\perp}|^2 - |A_{L\parallel}|^2 + |A_{R\perp}|^2 - |A_{R\parallel}|^2 \right], \\ I_4 &= \frac{1}{\sqrt{2}} \beta_l^2 \left[ \text{Re} \left( A_{L0} A_{L\parallel}^* \right) + \text{Re} \left( A_{R0} A_{R\parallel}^* \right) \right], \\ I_5 &= \sqrt{2} \beta_l \left[ \text{Re} \left( A_{L0} A_{L\perp}^* \right) - \text{Re} \left( A_{R0} A_{R\perp}^* \right) \right], \\ I_6 &= 2\beta_l \left[ \text{Re} \left( A_{L\parallel} A_{L\perp}^* \right) - \text{Re} \left( A_{R\parallel} A_{R\perp}^* \right) \right], \\ I_7 &= \sqrt{2} \beta_l \left[ \text{Im} \left( A_{L0} A_{L\parallel}^* \right) - \text{Im} \left( A_{R0} A_{R\parallel}^* \right) \right], \\ I_8 &= \frac{1}{\sqrt{2}} \beta_l^2 \left[ \text{Im} \left( A_{L0} A_{L\perp}^* \right) + \text{Im} \left( A_{R0} A_{R\perp}^* \right) \right], \\ I_9 &= \beta_l^2 \left[ \text{Im} \left( A_{L\parallel} A_{L\perp}^* \right) + \text{Im} \left( A_{R\parallel} A_{R\perp}^* \right) \right], \end{aligned} \quad (14)$$

where,  $\beta_l = \sqrt{1 - 4m_l^2/q^2}$  is the mass correction factor. For convenience, we introduce here the transversity amplitudes  $A_{L0}$ ,  $A_{R0}$ ,  $A_{L\perp}$ ,  $A_{R\perp}$ ,  $A_{L\parallel}$  and  $A_{R\parallel}$ . However, they are nothing but linear combinations of the helicity amplitudes as mentioned in the Ref. [18]. The subscripts  $L$  and  $R$  represent the chiralities of the lepton current where the right chiral amplitudes differ by left chiral amplitudes as  $A_{Ri} = A_{Li}|_{C_{10} \rightarrow -C_{10}}$ . In our analysis, we assume all the angular coefficients to be real and  $CP$  conserving. The explicit expressions for the transversity amplitudes for the

$B_s \rightarrow f'_2(1525)(\rightarrow K^+ K^-) \mu^+ \mu^-$  decay are written as follows:

$$\begin{aligned}
A_{L0} &= N_{f'_2} \frac{\sqrt{\lambda}}{\sqrt{6} m_{B_s} m_{f'_2}} \frac{1}{2 m_{f'_2} \sqrt{q^2}} \left\{ (C_9^{eff} - C_{10}) \left[ (m_{B_s}^2 - m_{f'_2}^2 - q^2)(m_{B_s} + m_{f'_2}) A_1 - \frac{\lambda}{m_{B_s} + m_{f'_2}} A_2 \right] + \right. \\
&\quad \left. 2 m_b C_7^{eff} \left[ (m_{B_s}^2 + 3 m_{f'_2}^2 - q^2) T_2 - \frac{\lambda}{m_{B_s}^2 - m_{f'_2}^2} T_3 \right] \right\} \\
A_{L\perp} &= -N_{f'_2} \sqrt{2} \frac{\sqrt{\lambda}}{\sqrt{8} m_{B_s} m_{f'_2}} \left[ (C_9^{eff} - C_{10}) \frac{\sqrt{\lambda}}{m_{B_s} + m_{f'_2}} V + \frac{\sqrt{\lambda} 2 m_b C_7^{eff}}{q^2} T_1 \right] \\
A_{L\parallel} &= N_{f'_2} \sqrt{2} \frac{\sqrt{\lambda}}{\sqrt{8} m_{B_s} m_{f'_2}} \left[ (C_9^{eff} - C_{10})(m_{B_s} + m_{f'_2}) A_1 + \frac{2 m_b C_7^{eff} (m_{B_s}^2 - m_{f'_2}^2)}{q^2} T_2 \right] \\
A_{Lt} &= N_{f'_2} \frac{\sqrt{\lambda}}{\sqrt{6} m_{B_s} m_{f'_2}} (C_9^{eff} - C_{10}) \frac{\sqrt{\lambda}}{\sqrt{q^2}} A_0
\end{aligned} \tag{15}$$

where,  $\lambda = m_{B_s}^4 + m_{f'_2}^4 + q^4 - 2(m_{B_s}^2 m_{f'_2}^2 + m_{f'_2}^2 q^2 + q^2 m_{B_s}^2)$  and  $N_{f'_2}$  is the normalization constant defined as

$$N_{f'_2} = \left[ \frac{G_F^2 \alpha_{em}^2}{3 \cdot 2^{10} \pi^5 m_{B_s}^3} |V_{tb} V_{ts}^*|^2 q^2 \sqrt{\lambda} \left( 1 - \frac{4m_l^2}{q^2} \right)^{1/2} \mathcal{B}(f'_2 \rightarrow K^+ K^-) \right]^{1/2}. \tag{16}$$

#### D. Decay distribution and other LFU observables

By integrating Eq. 13 with respect to  $\theta_K$ ,  $\theta_l$  and  $\phi$ , we obtain the differential decay rate. That is

$$\frac{d\Gamma}{dq^2} = \frac{1}{4} \left[ 3I_1^c + 6I_1^s - I_2^c - 2I_2^s \right] \tag{17}$$

We define several other  $q^2$  dependent observables such as the differential branching ratio, the longitudinal polarization fraction and the forward-backward asymmetry for the  $B_s \rightarrow f'_2(1525)(\rightarrow K^+ K^-) \mu^+ \mu^-$  decays. Those are

$$DBR(q^2) = \frac{d\Gamma/dq^2}{\Gamma_{Total}}, \quad F_L(q^2) = \frac{3I_1^c - I_2^c}{3I_1^c + 6I_1^s - I_2^c - 2I_2^s}, \quad A_{FB}(q^2) = \frac{3I_6}{3I_1^c + 6I_1^s - I_2^c - 2I_2^s} \tag{18}$$

In principle, the angular analysis of  $B_s \rightarrow f'_2(1525)(\rightarrow K^+ K^-) \mu^+ \mu^-$  decay provides several additional observables in the form of ratios of various angular coefficients. These observables are found to be very sensitive to NP. Here, we define some angular observables such as  $\langle P_1 \rangle$ ,  $\langle P_2 \rangle$ ,  $\langle P'_4 \rangle$  and  $\langle P'_5 \rangle$  as defined in Refs. [6, 7]. The explicit expressions are as follows:

$$\begin{aligned}
\langle P_1 \rangle &= \frac{1}{2} \frac{\int_{bin} dq^2 I_3}{\int_{bin} dq^2 I_2^s}, & \langle P_2 \rangle &= \frac{1}{8} \frac{\int_{bin} dq^2 I_6}{\int_{bin} dq^2 I_2^s}, & \langle P'_4 \rangle &= \frac{\int_{bin} dq^2 I_4}{\sqrt{-\int_{bin} dq^2 I_2^c \int_{bin} dq^2 I_2^s}}, & \langle P'_5 \rangle &= \frac{\int_{bin} dq^2 I_5}{2\sqrt{-\int_{bin} dq^2 I_2^c \int_{bin} dq^2 I_2^s}}
\end{aligned} \tag{19}$$

One can construct several other observables that can be defined in the form of ratios or in the form of differences between the observables involving two different families of lepton pairs. These observables such as the ratio of branching ratio  $R_{f'_2}$  and  $\langle Q_{FL} \rangle$ ,  $\langle Q_{AFB} \rangle$ ,  $\langle Q_i^{(\prime)} \rangle$  ( $i \in 1, 2, 4, 5$ ) are quite sensitive to NP. In the SM, we expect the value of  $R_{f'_2}$  to be very close to 1. Similarly, since the observables  $Q^{(\prime)}$  [36] are defined to be the differences between the  $e$  and  $\mu$  modes, one would expect these quantities to be almost zero in the SM. Hence any deviation from zero would be a clear signal of NP in  $b \rightarrow s l^+ l^-$  quark level transition decays. Measurement of these observables in future may provide crucial information regarding LFUV observed in various  $B$  meson decays. The explicit expressions for these observables are as follows:

$$R_{f'_2}(q^2) = \frac{\mathcal{B}(B_s \rightarrow f'_2 \mu^+ \mu^-)}{\mathcal{B}(B_s \rightarrow f'_2 e^+ e^-)} \tag{20}$$

and

$$\langle Q_{FL} \rangle = \langle F_L^\mu \rangle - \langle F_L^e \rangle, \quad \langle Q_{AFB} \rangle = \langle A_{FB}^\mu \rangle - \langle A_{FB}^e \rangle, \quad \langle Q_i^{(\prime)} \rangle = \langle P_i^{(\prime)\mu} \rangle - \langle P_i^{(\prime)e} \rangle. \tag{21}$$

### III. RESULTS AND DISCUSSIONS

#### A. Input Parameters

We report here all the relevant input parameters that are used in our numerical analysis. Masses of the mesons, leptons and quarks are in GeV, the Fermi coupling constant is in  $\text{GeV}^{-2}$  and the life time of  $B_s$  meson is in seconds. We consider the masses of  $b$  quark and  $c$  quark evaluated at the  $\overline{MS}$  scheme. The uncertainties associated with the CKM matrix element and  $\mathcal{B}(f_2' \rightarrow K^+ K^-)$  are reported within parentheses. We do not report the uncertainties associated with other input parameters as they are not important for our analysis. In Table III, we report the values of Wilson coefficients  $C_i(m_b)$  that are evaluated in the leading logarithmic approximation. The form factor input parameters evaluated in the pQCD approach are reported in Table IV where,  $F(0)$  denote the form factors at  $q^2 = 0$  i.e., at the maximum recoil point and  $a$  and  $b$  are the two fitted parameters. There are two kinds of errors associated with  $F(0)$ ,  $a$  and  $b$ . The first error is coming from the decay constant of the  $B_s$  meson and the shape parameter  $\omega_b$  and the second error is coming from the  $\Lambda_{QCD}$ , the scales  $ts$  and the threshold resummation parameter  $c$ . We refer to Ref. [34] for all the omitted details.

Parameter	Value	Parameter	Value	Parameter	Value	Parameter	Value	Parameter	Value
$m_{B_s}$	5.36689	$m_{f_2'}$	1.525	$m_b^{\overline{MS}}$	4.20	$m_c^{\overline{MS}}$	1.28	$m_b^{pole}$	4.80
$\tau_{B_s}$	$1.509 \times 10^{-12}$	$G_F$	$1.1663787 \times 10^{-5}$	$\alpha_e$	1/133.28	$ V_{tb}V_{ts}^* $	0.04088(55)	$\mathcal{B}(f_2' \rightarrow K^+ K^-)$	0.4435(11)

TABLE II: Theory input parameters [37]

$C_1$	$C_2$	$C_3$	$C_4$	$C_5$	$C_6$	$C_7^{eff}$	$C_9$	$C_{10}$
-0.248	1.107	0.011	-0.026	0.007	-0.031	-0.313	4.344	-4.669

TABLE III: Wilson coefficients  $C_i(m_b)$  in the leading logarithmic approximation [38]

	$V$	$A_0$	$A_1$	$T_1$	$T_2$	$T_3$
$F(0)$	$0.20_{-0.03-0.03}^{+0.04+0.05}$	$0.16_{-0.02-0.02}^{+0.03+0.03}$	$0.12_{-0.02-0.02}^{+0.02+0.03}$	$0.16_{-0.03-0.02}^{+0.03+0.04}$	$0.16_{-0.03-0.02}^{+0.03+0.04}$	$0.13_{-0.02-0.02}^{+0.03+0.03}$
$a$	$1.75_{-0.00-0.03}^{+0.02+0.05}$	$1.69_{-0.01-0.03}^{+0.00+0.04}$	$0.80_{-0.00-0.03}^{+0.02+0.07}$	$1.75_{-0.00-0.05}^{+0.01+0.05}$	$0.82_{-0.04-0.06}^{+0.00+0.04}$	$1.64_{-0.00-0.06}^{+0.02+0.06}$
$b$	$0.69_{-0.01-0.01}^{+0.05+0.08}$	$0.64_{-0.04-0.02}^{+0.00+0.01}$	$-0.11_{-0.00-0.00}^{+0.05+0.06}$	$0.71_{-0.01-0.08}^{+0.03+0.06}$	$-0.08_{-0.09-0.08}^{+0.00+0.03}$	$0.57_{-0.01-0.09}^{+0.04+0.05}$

TABLE IV: Form factor input parameters [34]

#### B. Standard Model predictions

We now proceed to discuss our results in the SM. We report in Table V and VI, the central values and the corresponding  $1\sigma$  uncertainties for each of the observables such as the differential branching ratio, the normalized longitudinal polarization fraction  $\langle F_L \rangle$ , the normalized forward-backward asymmetry  $\langle A_{FB} \rangle$ ,  $\langle P_1 \rangle$ ,  $\langle P_2 \rangle$ ,  $\langle P_4' \rangle$ ,  $\langle P_5' \rangle$  and also LFUV sensitive observables such as the ratio of branching ratio  $R_{f_2'}$ ,  $\langle Q_{F_L} \rangle$ ,  $\langle Q_{A_{FB}} \rangle$ ,  $\langle Q_i^{(l)} \rangle$  in different  $q^2$  bins for both  $e$  and the  $\mu$  mode. Here, we restrict our analysis to the low dilepton invariant mass region ranging from  $q^2 \in [0.045, 6.0]$   $\text{GeV}^2$  that excludes the charmonium contributions. We have considered several  $q^2$  bins with similar bin sizes such as  $[0.10, 0.98]$ ,  $[1.1, 2.5]$ ,  $[2.5, 4.0]$  and  $[4.0, 6.0]$  as reported by LHCb in the measurements of  $B_s \rightarrow \phi \mu^+ \mu^-$  decays [15, 16]. In addition, we include  $[1.1, 6.0]$  and  $[0.045, 6.0]$  bins as well. The central values for each observables are obtained by considering the central values of each input parameters. The corresponding  $1\sigma$  uncertainties are obtained by using the uncertainties associated with input parameters such as the form factors, the CKM matrix elements  $|V_{tb}V_{ts}^*|$  and the branching ratio of  $\mathcal{B}(f_2' \rightarrow K^+ K^-)$ . We notice here that the branching ratio for  $B_s \rightarrow f_2'(1525)(\rightarrow K^+ K^-) \{\mu^+/e^+\} \{\mu^-/e^-\}$  is of the order of  $\mathcal{O}(10^{-7})$  which is feasible with the currently available LHCb data. As expected, in the SM, both the  $e$  and  $\mu$  modes show similar behavior for all the observables.

Obviously, this is a clear confirmation of the LFU in the SM. To account for the LFU, we expect  $\langle Q_{F_L} \rangle$ ,  $\langle Q_{A_{FB}} \rangle$ ,  $\langle Q_i^{(j)} \rangle$ s ( $i \in 1, 2, 4, 5$ ) to be almost zero, although a slight non-zero contribution may occur due to the difference in the masses of  $e$  and  $\mu$ . In addition, we expect the ratio of branching ratio  $R_{f_2'}$  to be almost equal to unity. These are observed to be true from the entries reported in Table VII.

$q^2$ bins (GeV <sup>2</sup> )	BR $\times 10^{-7}$		$\langle F_L \rangle$		$\langle A_{FB} \rangle$	
	$e$ mode	$\mu$ mode	$e$ mode	$\mu$ mode	$e$ mode	$\mu$ mode
[0.10, 0.98]	0.116 $\pm$ 0.021	0.114 $\pm$ 0.021	0.502 $\pm$ 0.108	0.503 $\pm$ 0.108	0.096 $\pm$ 0.017	0.086 $\pm$ 0.016
[1.1, 2.5]	0.105 $\pm$ 0.025	0.105 $\pm$ 0.025	0.854 $\pm$ 0.043	0.855 $\pm$ 0.047	0.082 $\pm$ 0.034	0.082 $\pm$ 0.036
[2.5, 4.0]	0.111 $\pm$ 0.026	0.110 $\pm$ 0.026	0.841 $\pm$ 0.045	0.843 $\pm$ 0.045	-0.014 $\pm$ 0.040	-0.014 $\pm$ 0.039
[4.0, 6.0]	0.154 $\pm$ 0.035	0.153 $\pm$ 0.035	0.760 $\pm$ 0.062	0.762 $\pm$ 0.062	-0.116 $\pm$ 0.050	-0.116 $\pm$ 0.049
[1.1, 6.0]	0.370 $\pm$ 0.085	0.368 $\pm$ 0.085	0.810 $\pm$ 0.050	0.812 $\pm$ 0.050	-0.029 $\pm$ 0.040	-0.030 $\pm$ 0.040
[0.045, 6.0]	0.524 $\pm$ 0.103	0.512 $\pm$ 0.103	0.700 $\pm$ 0.071	0.712 $\pm$ 0.069	0.004 $\pm$ 0.030	-0.000 $\pm$ 0.030

TABLE V: The central values and the corresponding  $1\sigma$  uncertainties for each of the observables such as the branching ratio, the normalized longitudinal polarization fraction  $\langle F_L \rangle$ , the normalized forward-backward asymmetry  $\langle A_{FB} \rangle$  for both  $e$  mode and  $\mu$  mode of  $B_s \rightarrow f_2'(1525)(\rightarrow K^+ K^-) l^+ l^-$  decays.

$q^2$ bins (GeV <sup>2</sup> )	$\langle P_1 \rangle$		$\langle P_2 \rangle$		$\langle P_4' \rangle$		$\langle P_5' \rangle$	
	$e$ mode	$\mu$ mode	$e$ mode	$\mu$ mode	$e$ mode	$\mu$ mode	$e$ mode	$\mu$ mode
[0.10, 0.98]	-0.008 $\pm$ 0.265	-0.008 $\pm$ 0.267	0.132 $\pm$ 0.024	0.158 $\pm$ 0.029	-0.468 $\pm$ 0.086	-0.457 $\pm$ 0.089	0.554 $\pm$ 0.103	0.593 $\pm$ 0.114
[1.1, 2.5]	-0.043 $\pm$ 0.197	-0.043 $\pm$ 0.197	0.373 $\pm$ 0.080	0.378 $\pm$ 0.081	0.248 $\pm$ 0.234	0.251 $\pm$ 0.234	-0.076 $\pm$ 0.263	-0.079 $\pm$ 0.267
[2.5, 4.0]	-0.112 $\pm$ 0.240	-0.112 $\pm$ 0.240	-0.046 $\pm$ 0.157	-0.046 $\pm$ 0.158	0.810 $\pm$ 0.197	0.811 $\pm$ 0.197	-0.616 $\pm$ 0.235	-0.620 $\pm$ 0.236
[4.0, 6.0]	-0.159 $\pm$ 0.282	-0.159 $\pm$ 0.282	-0.314 $\pm$ 0.081	-0.315 $\pm$ 0.082	0.995 $\pm$ 0.156	0.995 $\pm$ 0.156	-0.794 $\pm$ 0.186	-0.797 $\pm$ 0.187
[1.1, 6.0]	-0.120 $\pm$ 0.221	-0.121 $\pm$ 0.222	-0.095 $\pm$ 0.128	-0.098 $\pm$ 0.128	0.735 $\pm$ 0.188	0.739 $\pm$ 0.188	-0.546 $\pm$ 0.219	-0.552 $\pm$ 0.220
[0.045, 6.0]	-0.060 $\pm$ 0.179	-0.074 $\pm$ 0.175	0.004 $\pm$ 0.067	-0.003 $\pm$ 0.085	0.307 $\pm$ 0.171	0.405 $\pm$ 0.183	-0.167 $\pm$ 0.185	-0.238 $\pm$ 0.204

TABLE VI: The central values and the corresponding  $1\sigma$  uncertainties of various angular observables such as  $\langle P_1 \rangle$ ,  $\langle P_2 \rangle$ ,  $\langle P_4' \rangle$ ,  $\langle P_5' \rangle$  for both  $e$  mode and  $\mu$  mode of  $B_s \rightarrow f_2'(1525)(\rightarrow K^+ K^-) l^+ l^-$  decays.

$q^2$ bins (GeV <sup>2</sup> )	$\langle R \rangle$	$\langle Q_1 \rangle$	$\langle Q_2 \rangle$	$\langle Q_4' \rangle$	$\langle Q_5' \rangle$	$\langle Q_{A_{FB}} \rangle$	$\langle Q_{F_L} \rangle$
[0.10, 0.98]	0.979 $\pm$ 0.005	0.000 $\pm$ 0.003	0.026 $\pm$ 0.005	0.011 $\pm$ 0.005	0.039 $\pm$ 0.011	-0.010 $\pm$ 0.002	0.001 $\pm$ 0.001
[1.1, 2.5]	0.994 $\pm$ 0.005	-0.000 $\pm$ 0.001	0.005 $\pm$ 0.002	0.002 $\pm$ 0.001	-0.002 $\pm$ 0.004	-0.002 $\pm$ 0.001	0.002 $\pm$ 0.001
[2.5, 4.0]	0.995 $\pm$ 0.005	-0.000 $\pm$ 0.000	-0.001 $\pm$ 0.001	0.000 $\pm$ 0.000	-0.004 $\pm$ 0.002	0.000 $\pm$ 0.001	0.002 $\pm$ 0.001
[4.0, 6.0]	0.996 $\pm$ 0.003	-0.000 $\pm$ 0.000	-0.001 $\pm$ 0.001	0.000 $\pm$ 0.000	-0.004 $\pm$ 0.001	0.001 $\pm$ 0.000	0.002 $\pm$ 0.000
[1.1, 6.0]	0.995 $\pm$ 0.002	-0.001 $\pm$ 0.002	-0.003 $\pm$ 0.001	0.004 $\pm$ 0.001	-0.007 $\pm$ 0.002	-0.000 $\pm$ 0.001	0.002 $\pm$ 0.001
[0.045, 6.0]	0.976 $\pm$ 0.005	-0.014 $\pm$ 0.040	-0.007 $\pm$ 0.019	0.098 $\pm$ 0.015	-0.071 $\pm$ 0.021	-0.004 $\pm$ 0.001	0.012 $\pm$ 0.002

TABLE VII: The central values and the corresponding  $1\sigma$  uncertainties of various LFUV sensitive observables such as the ratio of branching ratio  $\langle R_{f_2'} \rangle$ ,  $\langle Q_i^{(j)} \rangle$ ,  $\langle Q_{F_L} \rangle$ ,  $\langle Q_{A_{FB}} \rangle$  for  $B_s \rightarrow f_2'(1525)(\rightarrow K^+ K^-) l^+ l^-$  decays.

We show in Fig. 1 the  $q^2$  distribution of various observables in the low dilepton invariant mass region  $q^2 \in [0.045, 6.0]$  GeV<sup>2</sup>. The central line corresponds to the central values of each input parameters whereas to obtain the uncertainty band, we employ a naive  $\chi^2$  test on the input parameters. We define  $\chi^2$  as

$$\chi^2 = \sum_i \frac{(\mathcal{O}_i - \mathcal{O}_i^C)^2}{\Delta_i^2}, \quad (22)$$

where,  $\mathcal{O}_i \in (F(0), a, b, |V_{tb}V_{ts}^*|, \mathcal{B}(f_2' \rightarrow K^+ K^-))$  and  $\mathcal{O}_i^C$  represent the central values of each input parameters. Here  $\Delta_i$  represent the respective uncertainties associated with each input parameters. To obtain the uncertainty in each observable, we impose  $\chi^2 \leq 7.43$  constraint. From Fig. 1, we observe zero crossing in the  $q^2$  distribution of  $A_{FB}(q^2)$ ,  $P_2(q^2)$ ,  $P_4'(q^2)$ , and  $P_5'(q^2)$ . Interestingly, the  $A_{FB}(q^2)$  and  $P_2(q^2)$  have same zero crossing points i.e., at  $q^2 \sim 3_{-0.6}^{+0.8}$  GeV<sup>2</sup> and similarly, the  $P_4'(q^2)$  and  $P_5'(q^2)$  have the zero crossings at around  $q^2 \sim 1.4 \pm 0.3$  GeV<sup>2</sup> and  $q^2 \sim 1.6 \pm 0.4$  GeV<sup>2</sup>, respectively. Value of  $P_1(q^2)$  is almost zero in the low  $q^2$  region and becomes negative at higher  $q^2$  regions. The uncertainties associated with  $P_i^{(j)}(q^2)$  observables are more compared to  $DBR(q^2)$ ,  $F_L(q^2)$ , and  $A_{FB}(q^2)$ . The ratio of branching ratio  $R_{f_2'}(q^2)$  is almost equal to  $\sim 1$  in the whole  $q^2$  region and the uncertainty associated with  $R_{f_2'}(q^2)$  is quite negligible in comparison to the uncertainties present in other observables.

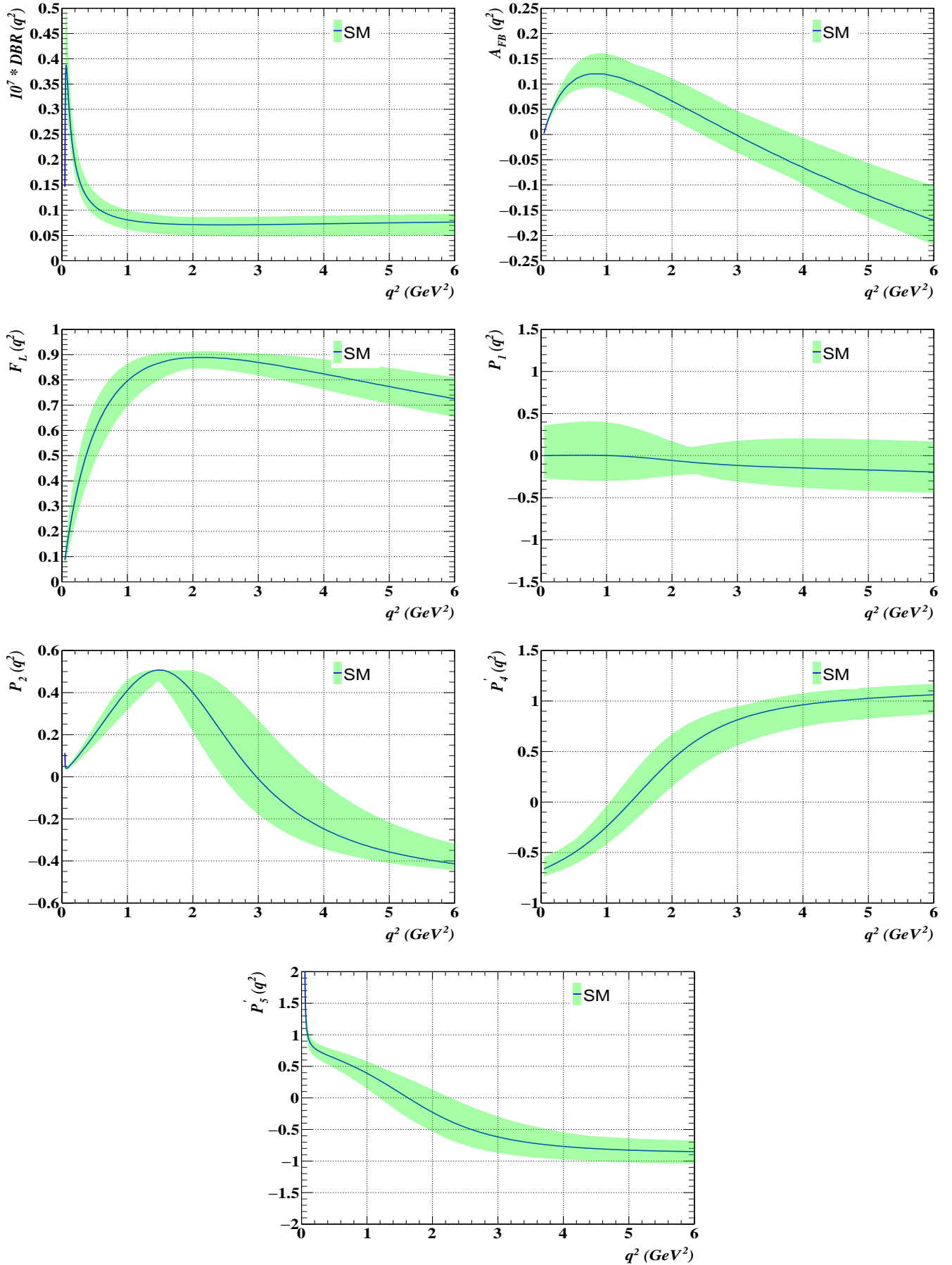


FIG. 1: The  $q^2$  distribution of various observables for the  $B_s \rightarrow f_2'(1525) \rightarrow K^+ K^- \mu^+ \mu^-$  decays in the SM. The band corresponds to the uncertainties in the input parameters such as the  $B_s \rightarrow f_2'$  transition form factors, CKM matrix element and  $\mathcal{B}(f_2' \rightarrow K^+ K^-)$ .

### C. New Physics

In order to explain the anomalies present in  $b \rightarrow s l^+ l^-$  transition decays, various global fits have been performed by several groups [39–47]. In principle, the NP can enter the effective Hamiltonian through several NP Lorentz structures such as vector, axial vector, scalar, pseudoscalar and tensor operators. But few measurements particularly,  $B_s \rightarrow \mu^+ \mu^-$  and  $b \rightarrow s \gamma$  put severe constraint on the scalar, pseudoscalar and tensor NP Lorentz structures [29–31] and hence they are omitted from our analysis. We refer to Ref. [32] for the global fit results that are performed on the new Wilson coefficients by considering  $C_{9,10}^{NP}$  and  $C'_{9,10}$ . In particular, these NP operators have V-A structure. The authors perform a global fit to these Wilson coefficients by using the constraints coming from observables such as  $R_K$ ,  $R_{K^*}$ ,  $P'_5$  and  $\mathcal{B}(B_s \rightarrow \phi \mu^+ \mu^-)$ . In addition, the fits also include the constraints coming from the branching ratio of  $B_s \rightarrow \mu^+ \mu^-$ , the differential branching ratio of  $B^0 \rightarrow K^{0*} \mu^+ \mu^-$ ,  $B^+ \rightarrow K^{+*} \mu^+ \mu^-$ ,  $B^0 \rightarrow K^0 \mu^+ \mu^-$ ,  $B^+ \rightarrow K^+ \mu^+ \mu^-$  and  $B \rightarrow X_s \mu^+ \mu^-$  in several  $q^2$  bins and also the constraints from the angular observables in  $B^0 \rightarrow K^{0*} \mu^+ \mu^-$  and  $B_s^0 \rightarrow \phi \mu^+ \mu^-$  decays in the several  $q^2$  bins. All the omitted details can be found in Ref. [32]. Out of various 1D and 2D scenarios, we consider total seven NP scenarios that are having high  $\Delta\chi^2$  values: four from 1D scenarios and three from 2D scenarios. We give bin wise predictions as well as the  $q^2$  distributions of various observables and make a comparative study among different NP scenarios and the SM for the  $B_s \rightarrow f'_2(1525)(\rightarrow K^+ K^-) l^+ l^-$  decay mode. The best fit values of the NP Wilson coefficients pertinent for our analysis taken from Ref. [32] are reported in Table VIII.

Wilson coefficients	$C_9^{NP}$	$C_{10}^{NP}$	$C_9^{NP} = -C_{10}^{NP}$	$C_9^{NP} = -C'_9$	$(C_9^{NP}, C_{10}^{NP})$	$(C_9^{NP} = -C'_9)$	$(C_9^{NP} = -C'_{10})$
Best fit values	-1.07	+0.78	-0.52	-1.11	(-0.94, +0.23)	(-1.27, +0.68)	(-1.36, -0.46)

TABLE VIII: Best fit values of NP Wilson coefficients [32]

#### 1. New Physics: 1D scenario

Let us now discuss the four 1D NP scenarios that arises due to contributions coming from  $C_9^{NP}$ ,  $C_{10}^{NP}$ ,  $C_9^{NP} = -C_{10}^{NP}$  and  $C_9^{NP} = -C'_9$ . The  $C_{9,10}^{NP}$  new Wilson coefficients are associated with similar interactions as that of  $C_{9,10}$  SM Wilson coefficients whereas,  $C'_{9,10}$  new Wilson coefficients arises due to the right chiral currents which are basically absent in the SM. We report in the Appendix in Tables IX, X, XI, XII, XIII, XIV, XV the average values of various observables such as the  $BR$ ,  $\langle F_L \rangle$ ,  $\langle A_{FB} \rangle$ ,  $\langle P_1 \rangle$ ,  $\langle P_2 \rangle$ ,  $\langle P'_4 \rangle$ ,  $\langle P'_5 \rangle$  for the  $\mu$  mode in several  $q^2$  bins. The corresponding bin wise plots have been displayed in Fig. 2. Our observations are as follows:

- $BR$ : In the first bin [0.045, 0.98], although the central values of all the NP scenarios differ slightly from the SM but they all lie within the SM  $1\sigma$  error band. In the bins [1.1, 2.5], [2.5, 4.0] and [4.0, 6.0], although the central values differ from the SM prediction, no significant deviations are observed, whereas, the central value obtained in case of  $C_9^{NP} = -C'_9$  NP scenario deviates by  $1 - 1.3\sigma$  from the SM expectations. This is true for the larger bin [1.1, 6.0] as well.
- $F_L$ : In the bin [0.045, 0.98], a deviation of around  $1\sigma$  from the SM prediction is observed for the  $C_9^{NP} = -C'_9$  NP scenario. For the rest of the NP scenarios, the deviation, however, is quite negligible. In the bin [1.1, 2.5], a deviation of around  $1.3\sigma$  and  $2.2\sigma$  from the SM prediction is observed in case of  $C_9^{NP}$  and  $C_9^{NP} = -C'_9$  NP scenarios, respectively. Similarly, in the bin [2.5, 4.0], the  $C_9^{NP} = -C'_9$  NP scenario shows a deviation of around  $1.5\sigma$  from the SM prediction. Moreover, in the bin [1.0, 6.0], a deviation of around  $1.5\sigma$  from the SM prediction is observed in case of  $C_9^{NP} = -C'_9$  NP scenario.
- $A_{FB}$ : In the bin [0.045, 0.98], the value of  $A_{FB}$  obtained in case of  $C_9^{NP} = -C'_9$  NP scenario lies outside the SM  $1\sigma$  error band, whereas, for rest of the NP scenarios, it seems to lie within the SM  $1\sigma$  error band. In the bin [1.1, 2.5], the  $C_{10}^{NP}$  is exactly like the SM, whereas,  $C_9^{NP}$  and  $C_9^{NP} = -C'_9$  show around  $1.5\sigma$  and  $2\sigma$  deviation from the SM prediction. In the bin [2.5, 4.0], a deviation of around  $1.4\sigma$  and  $1.6\sigma$  is observed in case of  $C_9^{NP}$  and  $C_9^{NP} = -C'_9$  NP scenarios, whereas, in case of  $C_{10}^{NP}$ , it is exactly like the SM.
- $P_1$ : Although the central values of  $P_1$  obtained in each NP scenarios differ from the SM central value, they, however, lie within the SM  $1\sigma$  error band and hence can not be distinguished from the SM predictions.

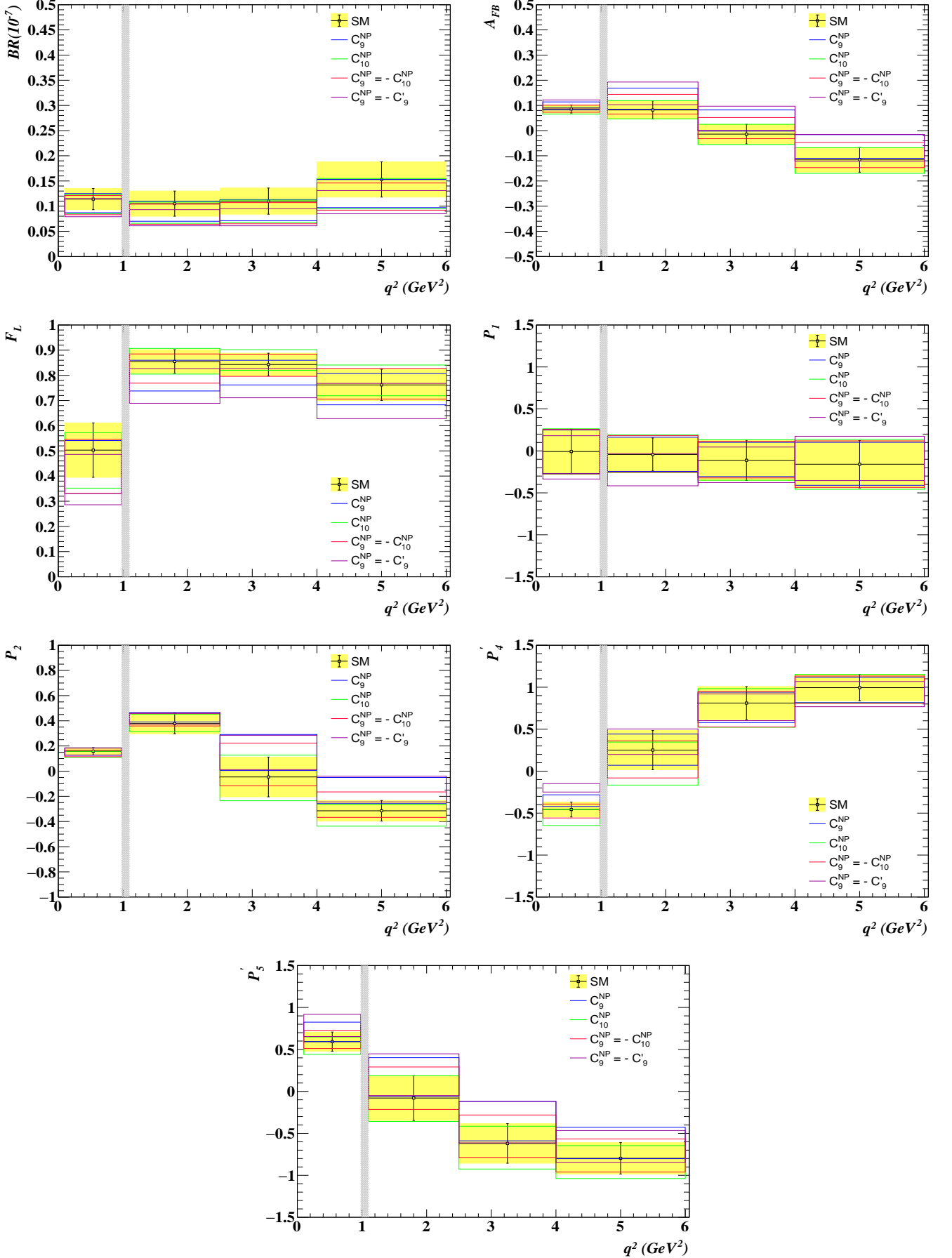


FIG. 2: The central values and the corresponding  $1\sigma$  error bands of various observables such as the branching ratio, the longitudinal polarization fraction  $F_L$ , the forward-backward asymmetry  $A_{FB}$ , and  $P_1$ ,  $P_2$ ,  $P_4$ ,  $P_5$  for the  $B_s \rightarrow f_2'(1525)(\rightarrow K^+ K^-) \mu^+ \mu^-$  decays in several  $q^2$  bins in the SM and in the presence of four 1D NP scenarios.

- $P_2$ : No significant deviations from the SM prediction are observed in the first two bins i.e., in  $[0.045, 0.98]$  and  $[1.1, 2.5]$ . However, in the bins  $[2.5, 4.0]$  and  $[4.0, 6.0]$ , the deviations observed in case of  $C_9^{NP}$  and  $C_9^{NP} = -C_9'$  NP scenarios are distinguishable from the SM prediction at the level of  $1.3\sigma$  and  $2\sigma$  significance.
- $P_4'$ : Although there is slight deviation in case of  $C_9^{NP}$  and  $C_{10}^{NP}$  NP scenarios, they, however, lie within the SM  $1\sigma$  error band in almost all  $q^2$  bins. Similarly, with  $C_9^{NP} = -C_{10}^{NP}$ , it is exactly SM like. With  $C_9^{NP} = -C_9'$  NP scenario, we observe a deviation of around  $2.5\sigma$  from the SM expectations in  $[0.045, 0.98]$  bin which is clearly distinguishable from the SM prediction.
- $P_5'$ : No significant deviation from the SM prediction is observed. The only exception is  $C_9^{NP} = -C_9'$  NP scenario in which a deviation of around  $1\sigma$  from the SM prediction is observed in the  $q^2 \in [0.045, 0.98]$  bin. It should be noted that the value of  $P_5'$  obtained with rest of the NP couplings lies within the SM error band.

We show in Fig 3 the  $q^2$  dependent observables for the  $B_s \rightarrow f_2'(1525) \mu^+ \mu^-$  decays in the presence of several NP WCs in 1D scenario. The SM error band is shown with green. The detailed observations are as follows:

- The differential branching ratio  $DBR(q^2)$  is slightly reduced at all  $q^2$  for each NP scenarios and it lies within the SM  $1\sigma$  error band.
- It is interesting to note that the zero crossing point of  $A_{FB}(q^2)$  is shifted towards the higher  $q^2$  regions than in the SM for most of the NP scenarios. It, however, coincides with the SM zero crossing point  $q^2 \sim 3_{-0.6}^{+0.8} \text{ GeV}^2$  for  $C_{10}^{NP}$  NP coupling. We observe the zero crossing of  $A_{FB}(q^2)$  at  $q^2 \sim 3.3 \text{ GeV}^2$  for  $C_9^{NP} = -C_{10}^{NP}$  scenario. Similarly, the zero crossing is observed at around  $q^2 \sim 3.8 \text{ GeV}^2$  for  $C_9^{NP}$  and  $C_9^{NP} = -C_9'$  NP scenarios, respectively. It is worth mentioning that the zero crossing points for  $C_9^{NP}$  and  $C_9^{NP} = -C_9'$  NP scenarios are distinguishable from the SM prediction at the level of  $1\sigma$  significance.
- For the longitudinal polarization fraction  $F_L(q^2)$ , the  $q^2$  distribution obtained for  $C_{10}^{NP}$  and  $C_9^{NP} = -C_{10}^{NP}$  NP scenarios is quite similar to that of the SM. In case of  $C_9^{NP}$ , it lies outside the SM error band in  $q^2 \in [1.1, 2.5]$  region and becomes very similar to the SM curve in the higher  $q^2$  regions. The maximum deviation from the SM prediction is observed for  $C_9^{NP} = -C_9'$  NP scenario.
- For the angular observable  $P_1(q^2)$ , the  $q^2$  distribution obtained for  $C_9^{NP}$ ,  $C_{10}^{NP}$  and  $C_9^{NP} = -C_{10}^{NP}$  NP scenarios is quite similar to the SM. The shape, however, is quite different from the SM in case of  $C_9^{NP} = -C_9'$  NP scenario. The value of  $P_1(q^2)$  obtained in this NP scenario is negative in the whole  $q^2$  region and reaches its minimum of around  $-0.25$  at  $q^2 = 2 \text{ GeV}^2$ .
- In the case of  $P_2(q^2)$ , similar to  $A_{FB}(q^2)$ , the zero crossing point is shifted towards the higher  $q^2$  regions than in the SM for most of the NP scenarios. The maximum deviation in the zero crossing point is observed in case of  $C_9^{NP}$  and  $C_9^{NP} = -C_9'$  NP scenarios, respectively.
- The angular observable  $P_4'(q^2)$  obtained in each of these 1D scenarios lies within the SM error band. There is, however, one exception. For  $C_9^{NP} = -C_9'$ , it lies outside the SM  $1\sigma$  error band in the low  $q^2$  region, i.e, for  $q^2 \leq 1 \text{ GeV}^2$ . In addition, the zero crossing points for the  $C_9^{NP} = -C_{10}^{NP}$  and  $C_{10}^{NP}$  NP scenarios are observed at  $q^2 \sim 1.5 \text{ GeV}^2$  and  $q^2 \sim 1.6 \text{ GeV}^2$ , whereas, the zero crossing points for  $C_9^{NP}$  and  $C_9^{NP} = -C_9'$  are observed at  $q^2 \sim 1.3 \text{ GeV}^2$  and  $q^2 \sim 1 \text{ GeV}^2$ , respectively. It is worth mentioning that the zero crossing point obtained in case of  $C_9^{NP} = -C_9'$  NP scenario is distinguishable from the SM zero crossing point  $q^2 \sim 1.4 \pm 0.3 \text{ GeV}^2$  at more than  $1\sigma$  significance.
- For the angular observable  $P_5'(q^2)$ , the zero crossing point obtained in each NP scenarios shifted towards the higher value of  $q^2$  than in the SM except for  $C_{10}^{NP}$ . In case of  $C_{10}^{NP}$ , the zero crossing point coincides with the SM zero crossing point of  $q^2 \sim 1.6 \pm 0.4 \text{ GeV}^2$ . For  $C_9^{NP} = -C_{10}^{NP}$  NP scenario, the zero crossing point is observed at  $q^2 \sim 1.8 \text{ GeV}^2$ , whereas, for  $C_9^{NP}$  and  $C_9^{NP} = -C_9'$  NP scenarios, we observe the zero crossing point at  $q^2 \sim 2.1 \text{ GeV}^2$  which deviates from the SM prediction at the level of around  $1\sigma$  significance.

## 2. New Physics: 2D scenario

Now we proceed to discuss the impact of several new Wilson coefficients from the 2D scenarios. We consider three different 2D scenarios:  $(C_9^{NP}, C_{10}^{NP})$ ,  $(C_9^{NP}, C_9')$  and  $(C_9^{NP}, C_{10}')$ . We report in the Appendix in the Tables IX, X, XI, XII, XIII, XIV, XV the average values of all the observables for the  $\mu$  mode. Similarly, the bin wise  $q^2$  distribution plots are shown in Fig. 4. The discussions pertaining to the impact of 2D new WC's on various observables are as follows:

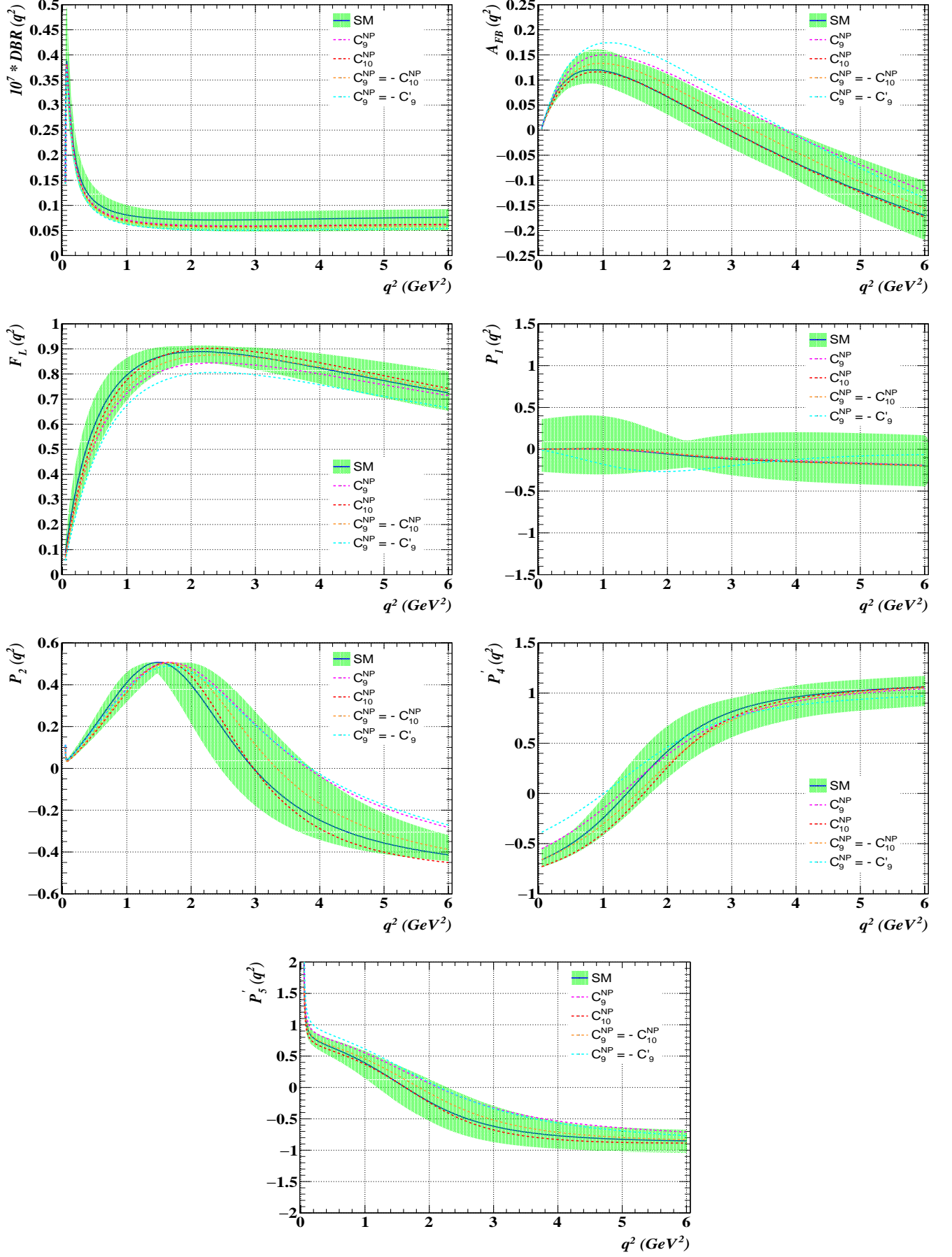


FIG. 3: The  $q^2$  distributions of various observables such as the differential branching ratio  $DBR(q^2)$ , the longitudinal polarization fraction  $F_L(q^2)$ , the forward-backward asymmetry  $A_{FB}(q^2)$ , and  $P_1(q^2)$ ,  $P_2(q^2)$ ,  $P_4'(q^2)$ ,  $P_5'(q^2)$  for the  $B_s \rightarrow f_2'(1525)(\rightarrow K^+ K^-) \mu^+ \mu^-$  decays in the SM and in the presence of  $C_9^{NP}$ ,  $C_{10}^{NP}$ ,  $C_9^{NP} = -C_{10}^{NP}$  and  $C_9^{NP} = -C_9'$  1D NP scenarios.

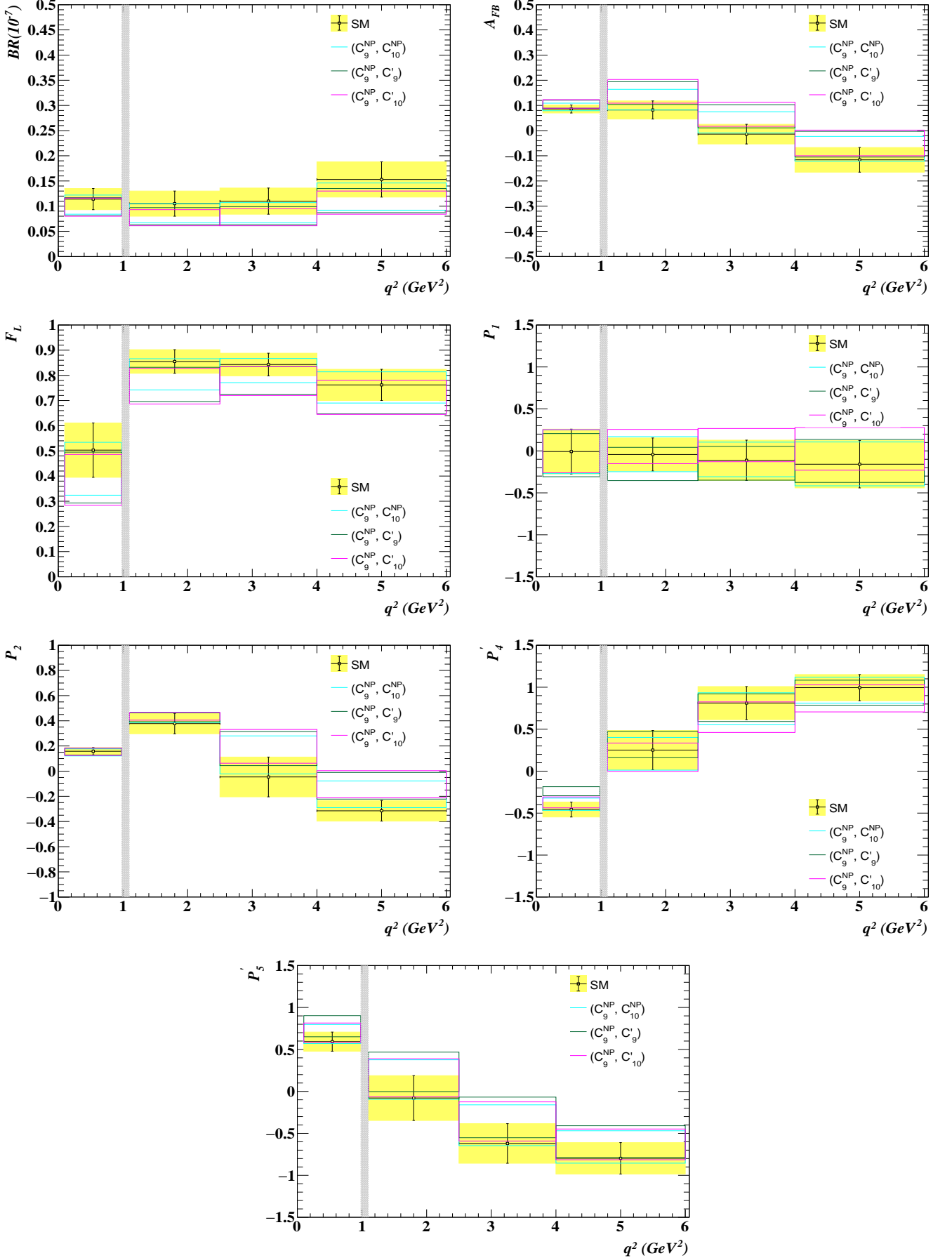


FIG. 4: The central values and the corresponding  $1\sigma$  error bands of various observables such as the branching ratio, the longitudinal polarization fraction  $F_L$ , the forward-backward asymmetry  $A_{FB}$ , and  $P_1$ ,  $P_2$ ,  $P_4$ ,  $P_5$  in several  $q^2$  bins for the  $B_s \rightarrow f_2'(1525) \rightarrow K^+ K^- \mu^+ \mu^-$  decays in the SM and in the presence of three 2D NP scenarios.

- $BR$ : Although the central values obtained for each NP scenarios differ from the SM prediction, no significant deviation is observed in any  $q^2$  bins. The deviation from the SM prediction is observed to be around  $1\sigma$  in case of  $(C_9^{NP}, C_9')$  and  $(C_9^{NP}, C'_{10})$  NP scenarios, whereas, for the  $(C_9^{NP}, C'_{10})$  NP scenario, the value of  $BR$  lies within the SM  $1\sigma$  error band.
- $F_L$ : In the bin  $q^2 \in [1.1, 2.5]$ , a deviation of around  $1.1\sigma$  from the SM prediction is observed in case of  $(C_9^{NP}, C_9')$  and  $(C_9^{NP}, C'_{10})$  NP scenarios. In all other  $q^2$  bins, the value of  $F_L$ , however, lies within the  $1\sigma$  SM error band for each NP scenarios.
- $A_{FB}$ : In the bin  $q^2 \in [1.1, 2.5]$  and  $q^2 \in [2.5, 4.0]$ , the deviation from the SM prediction is observed to be at  $1.1 - 1.2\sigma$  level in case of  $(C_9^{NP}, C_9')$  and  $(C_9^{NP}, C'_{10})$  NP scenarios. In all other bins, it however lies within the SM  $1\sigma$  error band for each NP scenarios.
- $P_1$ : Although the central values obtained for each NP scenarios differ from the SM central value, no significant deviation is observed as they all lie within the SM  $1\sigma$  error band.
- $P_2$ : A deviation of around  $1 - 1.1\sigma$  from the SM prediction is observed in the bin  $q^2 \in [2.5, 4.0]$  in case of  $(C_9^{NP}, C_9')$  and  $(C_9^{NP}, C'_{10})$  NP scenarios. Similarly, in the  $q^2 \in [4.0, 6.0]$  bin, a deviation of around  $1.5\sigma$  is observed in case of  $(C_9^{NP}, C_9')$  and  $(C_9^{NP}, C'_{10})$  NP scenarios.
- $P'_4$ : In the bin  $q^2 \in [0.045, 0.98]$ , the  $(C_9^{NP}, C_9')$  NP scenario is distinguishable from the SM prediction at the level of  $2\sigma$  significance, whereas, in case of  $(C_9^{NP}, C'_{10})$  and  $(C_9^{NP}, C'_{10})$  NP scenarios, the value of  $P'_4$  lies within the SM  $1\sigma$  error band and hence can not be distinguished from the SM prediction.
- $P'_5$ : In the bin  $q^2 \in [0.045, 0.98]$ , the value of  $P'_5$  obtained in case of  $(C_9^{NP}, C_9')$  NP scenario shows a deviation around  $1\sigma$  from the SM prediction, whereas, with other NP scenarios, it is consistent with the SM prediction. Similarly, in the bins  $q^2 \in [1.1, 2.5]$ ,  $[2.5, 4.0]$  and  $[4.0, 6.0]$ , no significant deviation from the SM prediction is observed and hence indistinguishable from the SM.

We show in Fig. 5 the  $q^2$  dependance of all the observables for the  $B_s \rightarrow f'_2(1525)\mu^+\mu^-$  decays in several  $2D$  scenarios. The SM  $1\sigma$  error band is shown with green. The detailed observations are as follows:

- Similar to the  $1D$  scenario, we observe that the differential branching ratio is slightly reduced at all  $q^2$  for each NP scenarios and they all lie within the SM error band.
- It is worth mentioning that the zero crossing point for  $A_{FB}(q^2)$  is shifted to higher  $q^2$  region for all the NP scenarios as compared to the SM. The zero crossing points for  $A_{FB}(q^2)$  are observed at  $q^2 \sim 3.6 \text{ GeV}^2$ ,  $q^2 \sim 4 \text{ GeV}^2$  and  $q^2 \sim 4.1 \text{ GeV}^2$  for  $(C_9^{NP}, C'_{10})$ ,  $(C_9^{NP}, C_9')$  and for  $(C_9^{NP}, C'_{10})$  NP scenarios, respectively. Although all the values are found to be distinct from the SM zero crossing point, it is important to note that the zero crossing point obtained in case of  $(C_9^{NP}, C_9')$  and  $(C_9^{NP}, C'_{10})$  NP scenarios are distinguishable from the SM prediction at the level of more than  $1\sigma$  significance.
- The peak of the longitudinal polarization fraction  $F_L(q^2)$  may shift towards higher  $q^2$  values than in the SM for each NP scenarios. It should be mentioned that the peak of  $F_L(q^2)$  obtained in case of  $(C_9^{NP}, C_9')$  and  $(C_9^{NP}, C'_{10})$  is distinguishable from the SM prediction at the level of more than  $1\sigma$  significance.
- The angular observable  $P_1(q^2)$  is zero in SM in the low  $q^2$  region, i.e, for  $q^2 \leq 1.2 \text{ GeV}^2$  and becomes negative as  $q^2$  increases. Similar behavior is observed in case of  $(C_9^{NP}, C'_{10})$  NP scenario as well. For  $(C_9^{NP}, C_9')$  NP scenario, it deviates slightly away from the SM and reaches minimum value of around  $-0.2$  at  $q^2 = 2 \text{ GeV}^2$ . However, we observe a completely different behavior in case of  $(C_9^{NP}, C'_{10})$  NP scenario. The value of  $P_1(q^2)$  acquires positive values in the whole  $q^2$  region and reaches its maximum value of  $0.1$  at  $q^2 \sim 2.2 \text{ GeV}^2$ . Since the SM error band is too large, the  $q^2$  distributions of all the NP scenarios lie within the SM error band.
- The peak of  $P_2(q^2)$  is slightly reduced and shifted towards the higher  $q^2$  values in each NP scenarios as compared to the SM. Moreover, the zero crossing point is also shifted to higher values of  $q^2$  than in the SM for all the NP scenarios. In case of  $(C_9^{NP}, C_9')$  and  $(C_9^{NP}, C'_{10})$  NP scenarios, the zero crossing points are distinguishable from the SM zero crossing at the level of more than  $1\sigma$  significance.
- For the angular observable  $P'_4(q^2)$ , no significant deviation from the SM is observed for each NP scenarios. However, in the low  $q^2$  region, i.e,  $q^2 \leq 1 \text{ GeV}^2$ , we see significant deviation of  $P'_4(q^2)$  from the SM prediction in case of  $(C_9^{NP}, C_9')$  NP scenario. Similarly, the zero crossing point of  $P'_4(q^2)$  obtained in case of  $(C_9^{NP}, C'_{10})$  and  $(C_9^{NP}, C'_{10})$  NP scenarios coincides with the SM zero crossing point of  $q^2 \sim 1.4 \pm 0.3 \text{ GeV}^2$ , whereas, for  $(C_9^{NP}, C_9')$  NP scenario, the zero crossing point is observed at  $q^2 \sim 1.1 \text{ GeV}^2$  and it is distinguishable from the SM zero crossing point at the level of  $1\sigma$  significance.

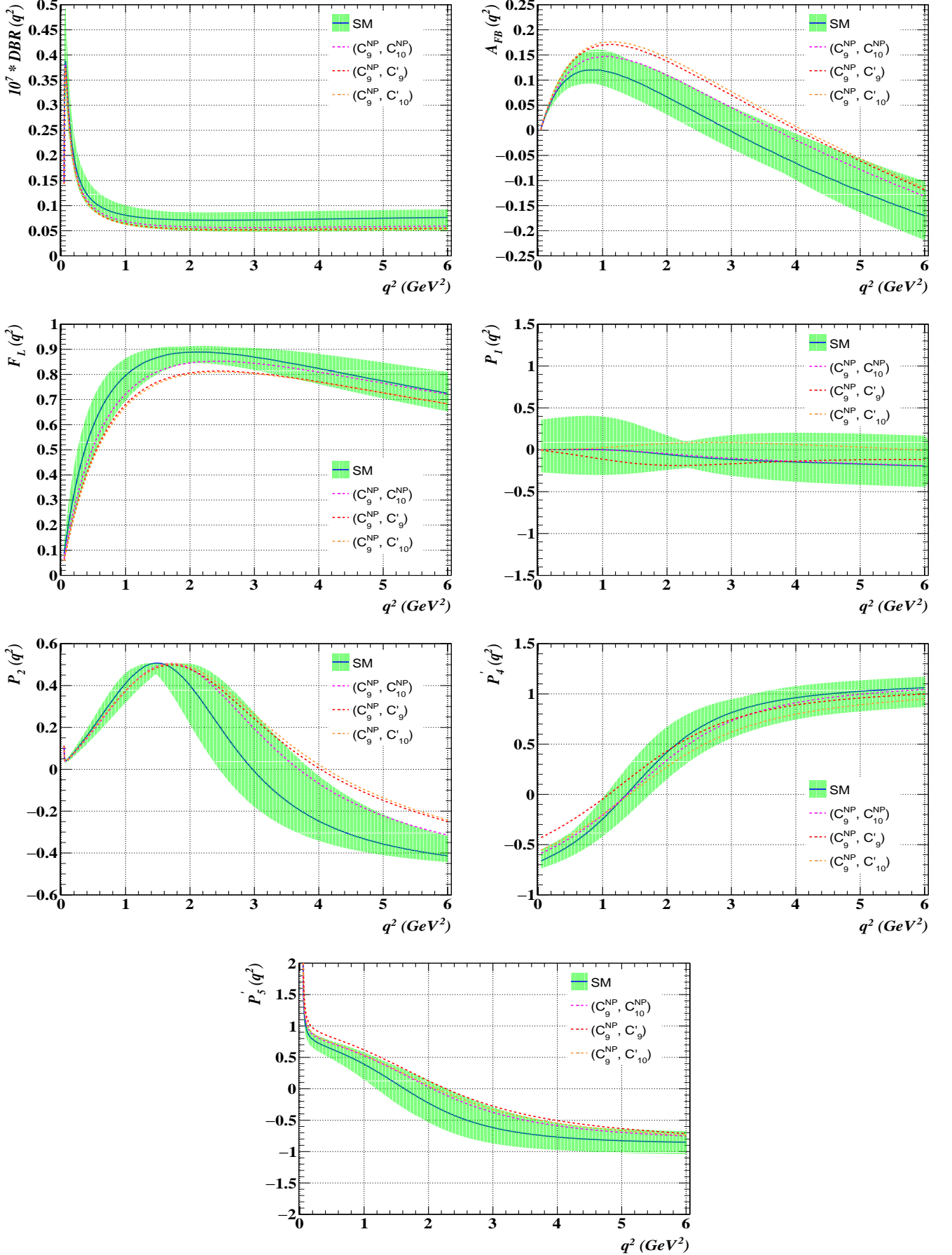


FIG. 5: The  $q^2$  distributions of various observables such as the differential branching ratio  $DBR(q^2)$ , the longitudinal polarization fraction  $F_L(q^2)$ , the forward-backward asymmetry  $A_{FB}(q^2)$ , and  $P_1(q^2)$ ,  $P_2(q^2)$ ,  $P_4(q^2)$ ,  $P_5(q^2)$  for the  $B_s \rightarrow f_2(1525) \rightarrow K^+ K^- \mu^+ \mu^-$  decays in the SM and in the presence of  $(C_9^{NP}, C_{10}^{NP})$ ,  $(C_9^{NP}, C_9')$  and  $(C_9^{NP}, C_{10}')$  2D NP scenarios.

- The  $q^2$  distribution of the angular observable  $P'_5(q^2)$  obtained in each NP scenarios is quite distinct from the SM. The maximum deviation from the SM prediction is observed for  $(C_9^{NP}, C'_9)$  NP scenario. The zero crossing points for all the three NP scenarios lie within  $q^2 \sim 2.1 - 2.3 \text{ GeV}^2$ , and interestingly, the zero crossing point for  $(C_9^{NP}, C'_9)$  is distinguishable from the SM at more than  $1.5\sigma$  significance.

#### D. Sensitivity of LFUV observables in $B_s \rightarrow f'_2(1525)(\rightarrow K^+ K^-)\mu^+ \mu^-$ decays

Study of LFUV in  $B_s \rightarrow f'_2(1525)(\rightarrow K^+ K^-)\mu^+ \mu^-$  decays is interesting because it is mediated via similar  $b \rightarrow s l^+ l^-$  quark level transition, and in principle, it can provide complementary information regarding the anomalies present in  $B \rightarrow (K, K^*)\mu^+ \mu^-$  decay modes. We study the violation of LFU in two different 1D and 2D NP scenarios. We make a comparative study of the LFUV sensitive observables such as  $\langle R_{f'_2} \rangle$ ,  $\langle Q_{FL} \rangle$ ,  $\langle Q_{A_{FB}} \rangle$ , and  $\langle Q_i^{(\prime)} \rangle$  ( $i \in 1, 2, 4, 5$ ) in the SM and in several 1D and 2D NP scenarios. We report in the Appendix in Tables XVI, XVII, XVIII, XIX, XX, XXI, XXII the binned average values of each of the observables. Similarly, the bin wise  $q^2$  distribution plots for both 1D and 2D scenarios are shown in Figs. 6 and 7, respectively. Our observations are as follows:

##### 1. 1D scenario

- $R_{f'_2}$ : Except in the low  $q^2$  bin, all the NP scenarios are distinguishable at more than  $5\sigma$  from the SM expectations. Hence, a measurement of  $R_{f'_2}$  will be crucial to probe NP in  $b \rightarrow s l^+ l^-$  transition decays.
- $Q_1$ : The value of  $Q_1$  obtained in case of  $C_9^{NP} = -C'_9$  NP scenario is distinguishable from the SM prediction at the level of  $4 - 5\sigma$  significance in the  $q^2 \in [0.045, 0.98]$  and  $[1.1, 2.5]$  bins. In the rest of the bins, although the central values obtained in each NP scenarios differ significantly from the SM, the SM band, however, overlaps with the NP band.
- $Q_2$ : The value of  $Q_2$  obtained in case of  $C_9^{NP}$  and  $C_9^{NP} = -C'_9$  NP scenarios are distinguishable from the SM prediction at the level of more than  $5\sigma$  significance in the region  $q^2 \in [2.5, 6.0]$ .
- $Q'_4$ : In the bin  $q^2 \in [1.1, 2.5]$ , the  $C_{10}^{NP}$  and  $C_9^{NP} = -C_{10}^{NP}$  NP scenarios are distinguishable at  $5 - 6\sigma$  from the SM. Although, the central values for  $C_9^{NP}$  and  $C_9^{NP} = -C'_9$  differ significantly from the SM expectations, the associated error band is too large and the SM band overlaps with the NP band. Similarly, for  $q^2 \geq 4$  the  $C_9^{NP} = -C'_9$  NP scenario is distinguishable at  $4.8\sigma$  from the SM expectations.
- $Q'_5$ : In the bin  $q^2 \in [1.1, 2.5]$ , the value of  $Q'_5$  obtained in case of  $C_9^{NP}$ ,  $C_9^{NP} = -C_{10}^{NP}$  and  $C_9^{NP} = -C'_9$  NP scenarios are clearly distinguishable from the SM prediction at more than  $5\sigma$  significance. Similarly, the  $C_9^{NP}$  and  $C_9^{NP} = -C'_9$  NP scenarios are distinguishable at more than  $3\sigma$  significance from the SM expectations for  $q^2 \leq 4 \text{ GeV}^2$ . For  $q^2 \geq 4 \text{ GeV}^2$ , the  $C_9^{NP}$  and  $C_9^{NP} = -C'_9$  NP scenarios are clearly distinguishable from the SM at the level of  $4.4\sigma$  and  $2.5\sigma$  significance, respectively.
- $Q_{A_{FB}}$ : The value of  $Q_{A_{FB}}$  obtained in case of  $C_9^{NP}$ ,  $C_9^{NP} = -C_{10}^{NP}$  and  $C_9^{NP} = -C'_9$  NP scenarios are clearly distinguishable from the SM prediction at the level of more than  $3\sigma$  significance, whereas, for the  $C_{10}^{NP}$  NP scenario, it is SM like.
- $Q_{FL}$ : In the low  $q^2$  region, the value of  $Q_{FL}$  deviates significantly from the SM prediction for all the NP scenarios and it is clearly distinguishable from the SM prediction at more than  $5\sigma$  significance. Similarly, for  $q^2 \geq 1$ , except for  $C_{10}^{NP}$ , the  $C_9^{NP}$ ,  $C_9^{NP} = -C_{10}^{NP}$  NP scenarios are distinguishable from the SM at the level of  $3\sigma$  significance.

##### 2. 2D scenario

- $R_{f'_2}$ : All the NP scenarios are distinguishable at more than  $3\sigma$  from the SM prediction and in particular, the deviation of  $R_{f'_2}$  from the SM prediction in case of  $(C_9^{NP}, C'_9)$  and  $(C_9^{NP}, C'_{10})$  NP scenarios are quite significant and it is clearly distinguishable from the SM prediction at more than  $5\sigma$  significance.
- $Q_1$ : The deviation observed in case of  $(C_9^{NP}, C'_{10})$  NP scenario is clearly distinguishable from the SM prediction at more than  $3\sigma$  significance in all  $q^2$  bins. Again, for  $(C_9^{NP}, C'_9)$  NP Scenario, although the central values differ

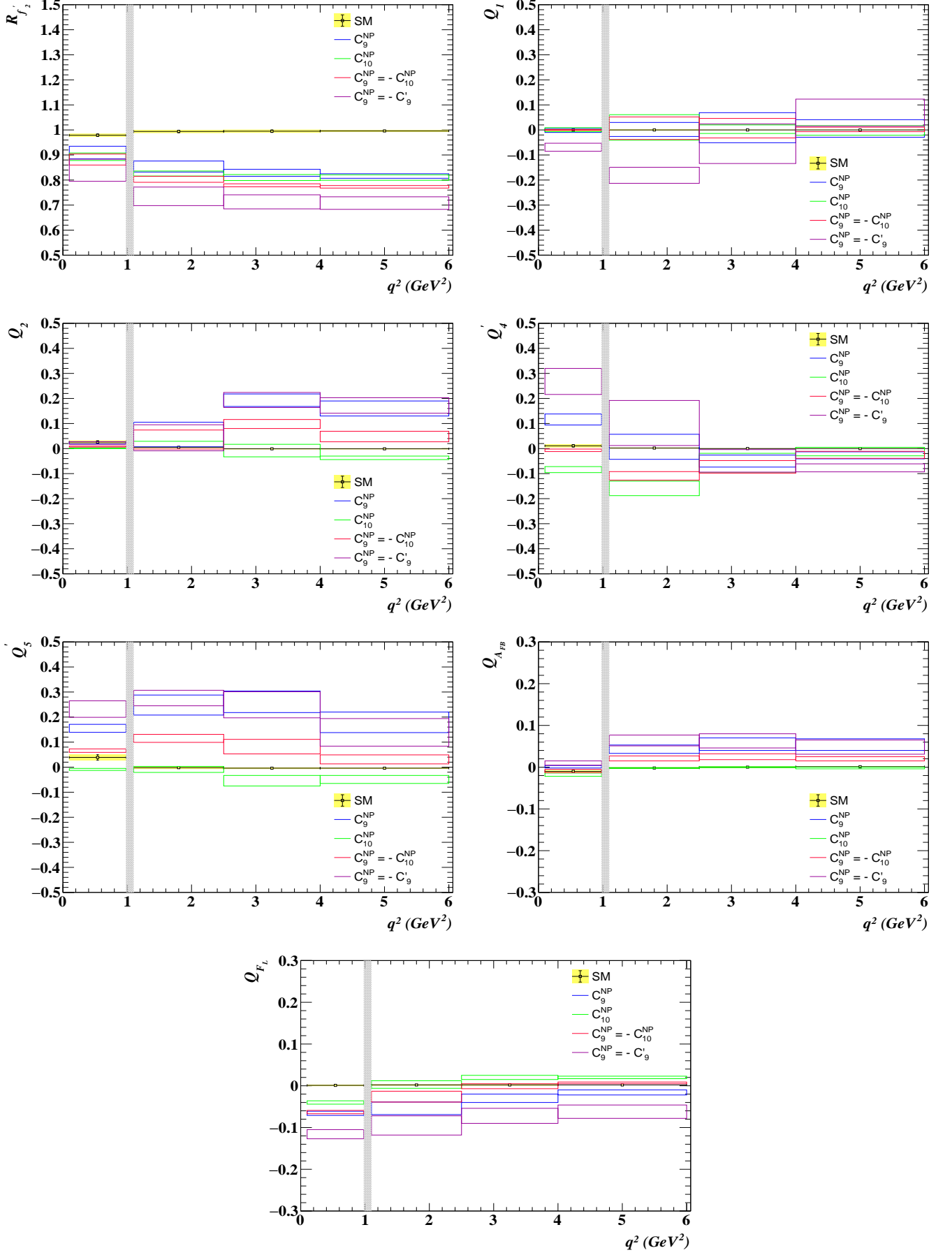


FIG. 6: The central values and the corresponding  $1\sigma$  error bands of various LFUV sensitive observables such as  $\langle R_{f_2} \rangle$ ,  $\langle Q_i^{(l)} \rangle$ ,  $\langle Q_{A_{FB}} \rangle$ , and  $\langle Q_{F_L} \rangle$  in several  $q^2$  bins in the SM and in the presence of four 1D NP scenarios.

significantly from the SM, the associated error band is too large in  $q^2 \geq 2.5$  bins and the SM value overlaps with the NP band.

- $Q_2$ : No significant deviation is found in  $q^2 \leq 2.5$  bins, whereas, for  $q^2 \geq 2.5$  bin, the deviation observed in case of  $(C_9^{NP}, C_9')$  and  $(C_9^{NP}, C_{10}')$  is quite significant and can be distinguishable from the SM prediction at more than  $5\sigma$  significance.
- $Q_4'$ : In the low  $q^2$  bin, the deviation observed in case of  $(C_9^{NP}, C_9')$  is clearly distinguishable from the SM prediction. In  $q^2 \in [2.5, 4.0]$  bin, the value of  $Q_4'$  obtained in case of  $(C_9^{NP}, C_{10}^{NP})$  is distinguishable from the SM prediction at  $3\sigma$  significance, whereas, in case of  $(C_9^{NP}, C_{10}')$  NP scenario, it is distinguishable at more than  $5\sigma$  significance. Similarly, in  $q^2 \geq 4$  bin,  $(C_9^{NP}, C_9')$  and  $(C_9^{NP}, C_{10}')$  NP scenarios are clearly distinguishable from the SM prediction at more than  $4\sigma$  significance.
- $Q_5'$ : Although the deviation from the SM prediction is observed to be more pronounced in case of  $(C_9^{NP}, C_9')$  NP scenario, the value of  $Q_5'$  obtained in each NP scenarios is clearly distinguishable from the SM prediction at more than  $5\sigma$  significance.
- $Q_{A_{FB}}$ : We observe significant deviation from the SM prediction for each NP scenarios. It should be noted that the value of  $Q_{A_{FB}}$  obtained in each NP scenarios is clearly distinguishable from the SM prediction at more than  $3\sigma$  significance.
- $Q_{F_L}$ : In the low  $q^2$  bin, all the three NP scenarios are clearly distinguishable from the SM at more than  $5\sigma$  significance. Similarly, for  $q^2 \geq 1$  bins, value of  $Q_{F_L}$  obtained in case of  $(C_9^{NP}, C_9')$  and  $(C_9^{NP}, C_{10}')$  NP scenarios is distinguishable from the SM prediction at more than  $3\sigma$  significance.

#### IV. CONCLUSION

In the light of the recent flavor anomalies reported in  $B \rightarrow (K, K^*)\mu^+\mu^-$  and  $B_s \rightarrow \phi\mu^+\mu^-$  decays, we analyze  $B_s \rightarrow f_2'(1525)\mu^+\mu^-$  decays mediated via similar  $b \rightarrow sl^+l^-$  neutral current quark level transition. We perform a detailed angular study of the four body differential decay of  $B_s \rightarrow f_2'(1525)(\rightarrow K^+K^-)\mu^+\mu^-$  within a model independent effective theory formalism. We give predictions of several observables in SM and in the presence of various 1D and 2D NP scenarios proposed in several global fits. In the SM, we obtain the branching ratio of  $B_s \rightarrow f_2'(1525)(\rightarrow K^+K^-)\mu^+\mu^-$  decays to be of the order of  $\mathcal{O}(10^{-7})$ . We observe that the branching ratio is reduced at all  $q^2$  for most of the NP cases. Except for  $C_{10}^{NP}$ , in all other NP scenarios, the zero crossing point for  $A_{FB}(q^2)$  is shifted to the higher  $q^2$  values than in the SM. In case of  $F_L$ , the peak seems to be reduced and shifted to the higher values of  $q^2$  in comparison to the SM. It is worth mentioning that the zero crossing for  $A_{FB}(q^2)$  is quite interesting and can, in principle, give useful information regarding lepton flavor universality violation in  $b \rightarrow sl^+l^-$  transition decays. Importantly, we do observe significant contributions coming from  $C_9^{NP} = -C_9'$  in the 1D scenario and  $(C_9^{NP}, C_9')$  and  $(C_9^{NP}, C_{10}')$  in the 2D scenario. Specially, these primed operators which corresponds to right handed currents seem to be very interesting. As expected, the lepton flavor universal ratio  $\langle R_{f_2'} \rangle$ , and other  $Q$  observables such as  $\langle Q_i^{(\prime)} \rangle$ ,  $\langle Q_{A_{FB}} \rangle$ , and  $\langle Q_{F_L} \rangle$  are exceptionally clean observable with theoretical uncertainty of only 1% which makes them ideal candidates to probe NP in  $b \rightarrow sl^+l^-$  transition decays. Although there have been several hints of NP reported in  $b \rightarrow sl^+l^-$  transition decays, but the existence of NP is yet to be confirmed. Unlike  $B \rightarrow (K, K^*)\mu^+\mu^-$  and  $B_s \rightarrow \phi\mu^+\mu^-$  decays which have caught more attention of the theorist and experimentalists, the  $B_s \rightarrow f_2'(1525)(\rightarrow K^+K^-)\mu^+\mu^-$  decays mediated via the same quark level transitions has received less attention so far. Measurements of various observables for this decay mode in future can shed more light in identifying the exact NP Lorentz structures. At the same time better theoretical understanding of the  $B_s \rightarrow f_2'$  transition form factors in future will be crucial in disentangling genuine NP effects from the SM uncertainties. More data samples are also needed in order to enhance the significance of the various measurements and to reduce the statistical and systematic uncertainties to properly disentangle the NP effects.

#### Acknowledgements

The author NS would like to thank Thomas Blake for several useful discussions.

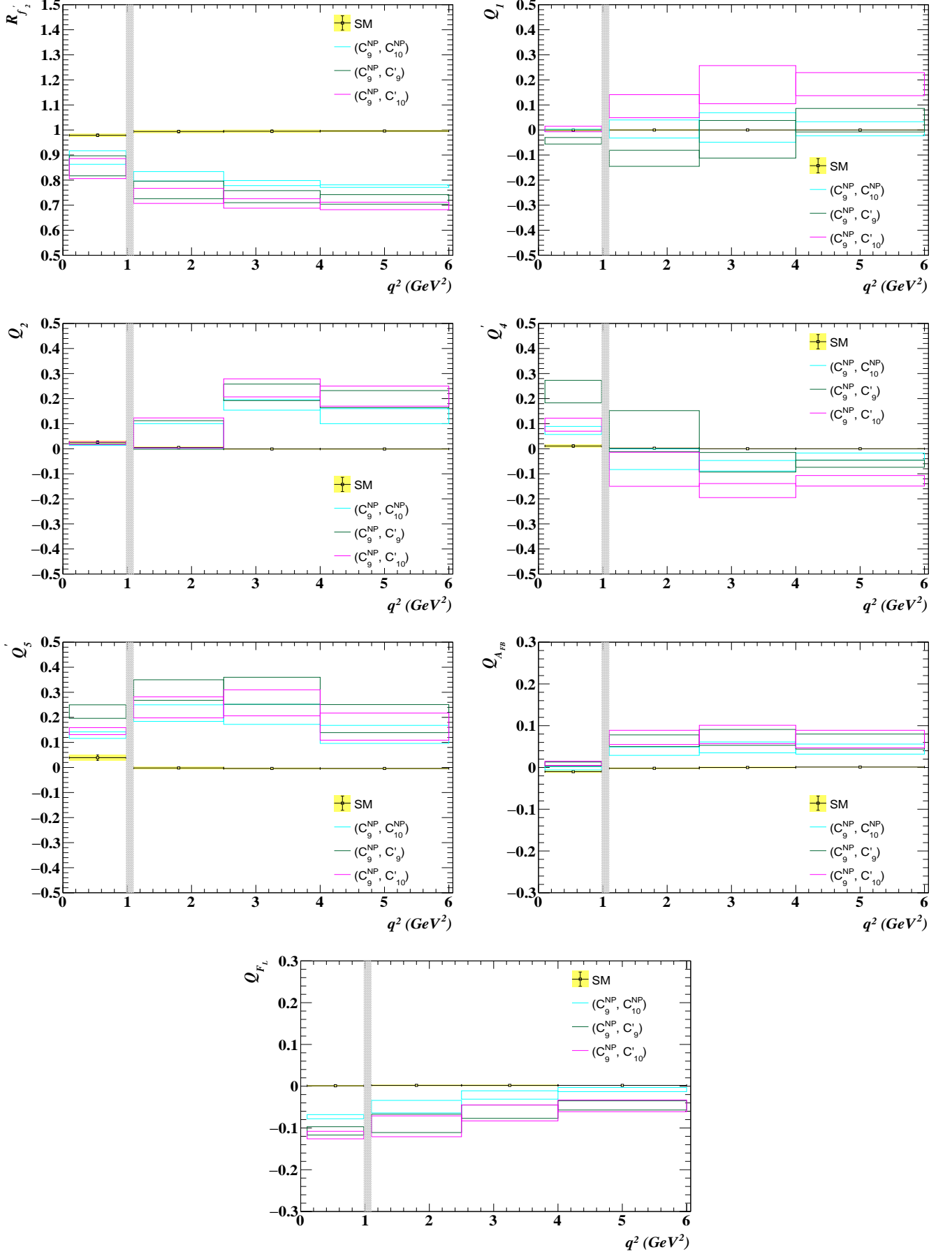


FIG. 7: The central values and the corresponding  $1\sigma$  error bands of various LFUV sensitive observables such as  $\langle R_{f_2} \rangle$ ,  $\langle Q_i^{(l)} \rangle$ ,  $\langle Q_{A_{FB}} \rangle$ , and  $\langle Q_{F_L} \rangle$  in several  $q^2$  bins in the SM and in the presence of three 2D NP scenarios.

**Appendix A: Predictions of various physical observables in the SM and in the presence various 1D and 2D NP couplings for the  $B_s \rightarrow f_2'(1525)(\rightarrow K^+ K^-) \mu^+ \mu^-$  decays**

$q^2$ bins (GeV <sup>2</sup> )	BR $\times 10^{-7}$							
	SM	$C_9^{NP}$	$C_{10}^{NP}$	$C_9^{NP} = -C_{10}^{NP}$	$C_9^{NP} = -C_9'$	$(C_9^{NP}, C_{10}^{NP})$	$(C_9^{NP}, C_9')$	$(C_9^{NP}, C_{10}')$
[0.10, 0.98]	0.114 $\pm$ 0.021	0.106 $\pm$ 0.019	0.104 $\pm$ 0.019	0.102 $\pm$ 0.019	0.097 $\pm$ 0.018	0.103 $\pm$ 0.019	0.099 $\pm$ 0.018	0.098 $\pm$ 0.018
[1.1, 2.5]	0.105 $\pm$ 0.025	0.090 $\pm$ 0.020	0.087 $\pm$ 0.021	0.084 $\pm$ 0.020	0.077 $\pm$ 0.016	0.086 $\pm$ 0.019	0.080 $\pm$ 0.017	0.077 $\pm$ 0.016
[2.5, 4.0]	0.110 $\pm$ 0.026	0.092 $\pm$ 0.021	0.090 $\pm$ 0.022	0.086 $\pm$ 0.021	0.078 $\pm$ 0.017	0.087 $\pm$ 0.020	0.081 $\pm$ 0.018	0.078 $\pm$ 0.017
[4.0, 6.0]	0.153 $\pm$ 0.035	0.125 $\pm$ 0.028	0.125 $\pm$ 0.030	0.119 $\pm$ 0.027	0.108 $\pm$ 0.023	0.119 $\pm$ 0.027	0.111 $\pm$ 0.024	0.107 $\pm$ 0.023
[1.1, 6.0]	0.368 $\pm$ 0.085	0.307 $\pm$ 0.068	0.302 $\pm$ 0.071	0.290 $\pm$ 0.067	0.264 $\pm$ 0.055	0.292 $\pm$ 0.065	0.271 $\pm$ 0.057	0.262 $\pm$ 0.056
[0.045, 6.0]	0.512 $\pm$ 0.103	0.440 $\pm$ 0.083	0.434 $\pm$ 0.086	0.420 $\pm$ 0.081	0.388 $\pm$ 0.068	0.423 $\pm$ 0.080	0.398 $\pm$ 0.071	0.387 $\pm$ 0.069

TABLE IX: The binned average central values and the corresponding  $1\sigma$  uncertainties for the branching ratio BR $\times 10^{-7}$  of  $B_s \rightarrow f_2'(1525)(\rightarrow K^+ K^-) \mu^+ \mu^-$  decays in the SM and in several NP cases.

$q^2$ bins (GeV <sup>2</sup> )	$\langle F_L \rangle$							
	SM	$C_9^{NP}$	$C_{10}^{NP}$	$C_9^{NP} = -C_{10}^{NP}$	$C_9^{NP} = -C_9'$	$(C_9^{NP}, C_{10}^{NP})$	$(C_9^{NP}, C_9')$	$(C_9^{NP}, C_{10}')$
[0.10, 0.98]	0.503 $\pm$ 0.108	0.436 $\pm$ 0.105	0.462 $\pm$ 0.110	0.439 $\pm$ 0.107	0.386 $\pm$ 0.100	0.429 $\pm$ 0.105	0.394 $\pm$ 0.101	0.385 $\pm$ 0.101
[1.1, 2.5]	0.855 $\pm$ 0.047	0.799 $\pm$ 0.061	0.856 $\pm$ 0.051	0.827 $\pm$ 0.058	0.758 $\pm$ 0.069	0.804 $\pm$ 0.062	0.764 $\pm$ 0.068	0.757 $\pm$ 0.071
[2.5, 4.0]	0.843 $\pm$ 0.045	0.811 $\pm$ 0.049	0.861 $\pm$ 0.041	0.840 $\pm$ 0.044	0.769 $\pm$ 0.058	0.819 $\pm$ 0.048	0.780 $\pm$ 0.055	0.777 $\pm$ 0.057
[4.0, 6.0]	0.762 $\pm$ 0.062	0.745 $\pm$ 0.062	0.780 $\pm$ 0.061	0.767 $\pm$ 0.061	0.698 $\pm$ 0.070	0.752 $\pm$ 0.062	0.714 $\pm$ 0.067	0.713 $\pm$ 0.068
[1.1, 6.0]	0.812 $\pm$ 0.050	0.779 $\pm$ 0.054	0.825 $\pm$ 0.047	0.805 $\pm$ 0.050	0.735 $\pm$ 0.062	0.786 $\pm$ 0.053	0.747 $\pm$ 0.060	0.744 $\pm$ 0.061
[0.045, 6.0]	0.712 $\pm$ 0.069	0.662 $\pm$ 0.077	0.700 $\pm$ 0.074	0.677 $\pm$ 0.077	0.611 $\pm$ 0.081	0.662 $\pm$ 0.078	0.622 $\pm$ 0.080	0.615 $\pm$ 0.083

TABLE X: The binned average central values and the corresponding  $1\sigma$  uncertainties for the normalized longitudinal polarization fraction  $\langle F_L \rangle$  of  $B_s \rightarrow f_2'(1525)(\rightarrow K^+ K^-) \mu^+ \mu^-$  decays in the SM and in several NP cases.

$q^2$ bins (GeV <sup>2</sup> )	$\langle A_{FB} \rangle$							
	SM	$C_9^{NP}$	$C_{10}^{NP}$	$C_9^{NP} = -C_{10}^{NP}$	$C_9^{NP} = -C_9'$	$(C_9^{NP}, C_{10}^{NP})$	$(C_9^{NP}, C_9')$	$(C_9^{NP}, C_{10}')$
[0.10, 0.98]	0.086 $\pm$ 0.016	0.098 $\pm$ 0.016	0.079 $\pm$ 0.013	0.087 $\pm$ 0.014	0.106 $\pm$ 0.016	0.094 $\pm$ 0.015	0.105 $\pm$ 0.016	0.106 $\pm$ 0.017
[1.1, 2.5]	0.082 $\pm$ 0.036	0.127 $\pm$ 0.042	0.083 $\pm$ 0.036	0.105 $\pm$ 0.039	0.148 $\pm$ 0.045	0.123 $\pm$ 0.041	0.149 $\pm$ 0.045	0.156 $\pm$ 0.047
[2.5, 4.0]	-0.014 $\pm$ 0.039	0.040 $\pm$ 0.042	-0.015 $\pm$ 0.040	0.010 $\pm$ 0.042	0.049 $\pm$ 0.048	0.033 $\pm$ 0.042	0.057 $\pm$ 0.046	0.065 $\pm$ 0.048
[4.0, 6.0]	-0.116 $\pm$ 0.049	-0.063 $\pm$ 0.047	-0.119 $\pm$ 0.051	-0.097 $\pm$ 0.050	-0.068 $\pm$ 0.053	-0.072 $\pm$ 0.049	-0.054 $\pm$ 0.051	-0.049 $\pm$ 0.051
[1.1, 6.0]	-0.030 $\pm$ 0.040	0.023 $\pm$ 0.041	-0.030 $\pm$ 0.040	-0.007 $\pm$ 0.041	0.029 $\pm$ 0.046	0.016 $\pm$ 0.041	0.038 $\pm$ 0.044	0.045 $\pm$ 0.046
[0.045, 6.0]	-0.000 $\pm$ 0.030	0.042 $\pm$ 0.030	-0.000 $\pm$ 0.030	0.019 $\pm$ 0.030	0.048 $\pm$ 0.032	0.036 $\pm$ 0.030	0.054 $\pm$ 0.031	0.059 $\pm$ 0.032

TABLE XI: The binned average central values and the corresponding  $1\sigma$  uncertainties for the normalized forward-backward asymmetry  $\langle A_{FB} \rangle$  of  $B_s \rightarrow f_2'(1525)(\rightarrow K^+ K^-) \mu^+ \mu^-$  decays in the SM and in several NP cases.

$q^2$ bins (GeV <sup>2</sup> )	$\langle P_1 \rangle$							
	SM	$C_9^{NP}$	$C_{10}^{NP}$	$C_9^{NP} = -C_{10}^{NP}$	$C_9^{NP} = -C_9'$	$(C_9^{NP}, C_{10}^{NP})$	$(C_9^{NP}, C_9')$	$(C_9^{NP}, C_{10}')$
[0.10, 0.98]	-0.008 $\pm$ 0.267	-0.010 $\pm$ 0.259	-0.007 $\pm$ 0.270	-0.009 $\pm$ 0.265	-0.077 $\pm$ 0.258	-0.010 $\pm$ 0.261	-0.051 $\pm$ 0.257	-0.004 $\pm$ 0.257
[1.1, 2.5]	-0.043 $\pm$ 0.197	-0.041 $\pm$ 0.203	-0.034 $\pm$ 0.224	-0.036 $\pm$ 0.217	-0.224 $\pm$ 0.192	-0.039 $\pm$ 0.209	-0.156 $\pm$ 0.198	0.052 $\pm$ 0.204
[2.5, 4.0]	-0.112 $\pm$ 0.240	-0.102 $\pm$ 0.204	-0.109 $\pm$ 0.241	-0.104 $\pm$ 0.218	-0.166 $\pm$ 0.212	-0.102 $\pm$ 0.206	-0.148 $\pm$ 0.201	0.069 $\pm$ 0.198
[4.0, 6.0]	-0.159 $\pm$ 0.282	-0.154 $\pm$ 0.256	-0.161 $\pm$ 0.297	-0.158 $\pm$ 0.277	-0.090 $\pm$ 0.264	-0.155 $\pm$ 0.261	-0.120 $\pm$ 0.256	0.024 $\pm$ 0.254
[1.1, 6.0]	-0.121 $\pm$ 0.222	-0.110 $\pm$ 0.196	-0.117 $\pm$ 0.219	-0.112 $\pm$ 0.204	-0.141 $\pm$ 0.201	-0.110 $\pm$ 0.196	-0.135 $\pm$ 0.193	0.043 $\pm$ 0.193
[0.045, 6.0]	-0.074 $\pm$ 0.175	-0.067 $\pm$ 0.177	-0.066 $\pm$ 0.178	-0.064 $\pm$ 0.179	-0.106 $\pm$ 0.176	-0.065 $\pm$ 0.178	-0.094 $\pm$ 0.176	0.024 $\pm$ 0.178

TABLE XII: The binned average central values and the corresponding  $1\sigma$  uncertainties for  $\langle P_1 \rangle$  of  $B_s \rightarrow f_2'(1525)(\rightarrow K^+ K^-) \mu^+ \mu^-$  decays in the SM and in several NP cases.

$q^2$ bins (GeV <sup>2</sup> )	$\langle P_2 \rangle$							
	SM	$C_9^{NP}$	$C_{10}^{NP}$	$C_9^{NP} = -C_{10}^{NP}$	$C_9^{NP} = -C_9'$	$(C_9^{NP}, C_{10}^{NP})$	$(C_9^{NP}, C_9')$	$(C_9^{NP}, C_{10}')$
[0.10, 0.98]	$0.158 \pm 0.029$	$0.156 \pm 0.029$	$0.133 \pm 0.025$	$0.141 \pm 0.026$	$0.155 \pm 0.028$	$0.149 \pm 0.028$	$0.155 \pm 0.028$	$0.154 \pm 0.029$
[1.1, 2.5]	$0.378 \pm 0.081$	$0.429 \pm 0.038$	$0.383 \pm 0.070$	$0.409 \pm 0.050$	$0.416 \pm 0.042$	$0.425 \pm 0.039$	$0.428 \pm 0.035$	$0.436 \pm 0.031$
[2.5, 4.0]	$-0.046 \pm 0.158$	$0.148 \pm 0.143$	$-0.054 \pm 0.181$	$0.053 \pm 0.169$	$0.148 \pm 0.136$	$0.129 \pm 0.151$	$0.179 \pm 0.135$	$0.197 \pm 0.134$
[4.0, 6.0]	$-0.315 \pm 0.082$	$-0.154 \pm 0.104$	$-0.351 \pm 0.086$	$-0.266 \pm 0.101$	$-0.142 \pm 0.102$	$-0.184 \pm 0.106$	$-0.116 \pm 0.106$	$-0.104 \pm 0.108$
[1.1, 6.0]	$-0.098 \pm 0.128$	$0.072 \pm 0.119$	$-0.109 \pm 0.141$	$-0.019 \pm 0.135$	$0.076 \pm 0.115$	$0.052 \pm 0.125$	$0.103 \pm 0.114$	$0.118 \pm 0.113$
[0.045, 6.0]	$-0.003 \pm 0.085$	$0.098 \pm 0.063$	$-0.006 \pm 0.084$	$0.044 \pm 0.074$	$0.100 \pm 0.062$	$0.085 \pm 0.066$	$0.116 \pm 0.058$	$0.124 \pm 0.056$

TABLE XIII: The binned average central values and the corresponding  $1\sigma$  uncertainties for  $\langle P_2 \rangle$  of  $B_s \rightarrow f_2'(1525)(\rightarrow K^+ K^-) \mu^+ \mu^-$  decays in the SM and in several NP cases.

$q^2$ bins (GeV <sup>2</sup> )	$\langle P_4' \rangle$							
	SM	$C_9^{NP}$	$C_{10}^{NP}$	$C_9^{NP} = -C_{10}^{NP}$	$C_9^{NP} = -C_9'$	$(C_9^{NP}, C_{10}^{NP})$	$(C_9^{NP}, C_9')$	$(C_9^{NP}, C_{10}')$
[0.10, 0.98]	$-0.457 \pm 0.089$	$-0.351 \pm 0.069$	$-0.552 \pm 0.095$	$-0.475 \pm 0.083$	$-0.199 \pm 0.050$	$-0.394 \pm 0.073$	$-0.239 \pm 0.054$	$-0.372 \pm 0.065$
[1.1, 2.5]	$0.251 \pm 0.234$	$0.256 \pm 0.186$	$0.090 \pm 0.256$	$0.140 \pm 0.221$	$0.351 \pm 0.152$	$0.207 \pm 0.195$	$0.318 \pm 0.158$	$0.166 \pm 0.169$
[2.5, 4.0]	$0.811 \pm 0.197$	$0.760 \pm 0.181$	$0.753 \pm 0.230$	$0.737 \pm 0.211$	$0.761 \pm 0.159$	$0.743 \pm 0.191$	$0.756 \pm 0.164$	$0.643 \pm 0.182$
[4.0, 6.0]	$0.995 \pm 0.156$	$0.968 \pm 0.150$	$0.983 \pm 0.170$	$0.970 \pm 0.163$	$0.918 \pm 0.150$	$0.964 \pm 0.155$	$0.935 \pm 0.149$	$0.867 \pm 0.161$
[1.1, 6.0]	$0.739 \pm 0.188$	$0.702 \pm 0.173$	$0.668 \pm 0.215$	$0.666 \pm 0.199$	$0.707 \pm 0.152$	$0.681 \pm 0.182$	$0.703 \pm 0.157$	$0.597 \pm 0.173$
[0.045, 6.0]	$0.405 \pm 0.183$	$0.395 \pm 0.161$	$0.297 \pm 0.198$	$0.320 \pm 0.181$	$0.439 \pm 0.135$	$0.361 \pm 0.167$	$0.423 \pm 0.141$	$0.315 \pm 0.152$

TABLE XIV: The binned average central values and the corresponding  $1\sigma$  uncertainties for  $\langle P_4' \rangle$  of  $B_s \rightarrow f_2'(1525)(\rightarrow K^+ K^-) \mu^+ \mu^-$  decays in the SM and in several NP cases.

$q^2$ bins (GeV <sup>2</sup> )	$\langle P_5' \rangle$							
	SM	$C_9^{NP}$	$C_{10}^{NP}$	$C_9^{NP} = -C_{10}^{NP}$	$C_9^{NP} = -C_9'$	$(C_9^{NP}, C_{10}^{NP})$	$(C_9^{NP}, C_9')$	$(C_9^{NP}, C_{10}')$
[0.10, 0.98]	$0.593 \pm 0.114$	$0.709 \pm 0.116$	$0.545 \pm 0.104$	$0.620 \pm 0.109$	$0.786 \pm 0.132$	$0.684 \pm 0.114$	$0.777 \pm 0.126$	$0.700 \pm 0.115$
[1.1, 2.5]	$-0.079 \pm 0.267$	$0.172 \pm 0.230$	$-0.086 \pm 0.272$	$0.038 \pm 0.253$	$0.199 \pm 0.249$	$0.141 \pm 0.236$	$0.233 \pm 0.235$	$0.163 \pm 0.226$
[2.5, 4.0]	$-0.620 \pm 0.236$	$-0.354 \pm 0.23$	$-0.670 \pm 0.255$	$-0.534 \pm 0.253$	$-0.366 \pm 0.247$	$-0.403 \pm 0.243$	$-0.310 \pm 0.242$	$-0.358 \pm 0.233$
[4.0, 6.0]	$-0.797 \pm 0.187$	$-0.615 \pm 0.187$	$-0.842 \pm 0.196$	$-0.763 \pm 0.197$	$-0.655 \pm 0.189$	$-0.662 \pm 0.193$	$-0.599 \pm 0.190$	$-0.631 \pm 0.183$
[1.1, 6.0]	$-0.552 \pm 0.220$	$-0.316 \pm 0.219$	$-0.580 \pm 0.232$	$-0.469 \pm 0.233$	$-0.329 \pm 0.233$	$-0.358 \pm 0.226$	$-0.277 \pm 0.227$	$-0.322 \pm 0.219$
[0.045, 6.0]	$-0.238 \pm 0.204$	$-0.036 \pm 0.194$	$-0.237 \pm 0.204$	$-0.148 \pm 0.203$	$-0.029 \pm 0.211$	$-0.064 \pm 0.198$	$0.008 \pm 0.202$	$-0.041 \pm 0.195$

TABLE XV: The binned average central values and the corresponding  $1\sigma$  uncertainties for  $\langle P_5' \rangle$  of  $B_s \rightarrow f_2'(1525)(\rightarrow K^+ K^-) \mu^+ \mu^-$  decays in the SM and in several NP cases.

$q^2$ bins (GeV <sup>2</sup> )	$\langle R_{f_2'} \rangle$							
	SM	$C_9^{NP}$	$C_{10}^{NP}$	$C_9^{NP} = -C_{10}^{NP}$	$C_9^{NP} = -C_9'$	$(C_9^{NP}, C_{10}^{NP})$	$(C_9^{NP}, C_9')$	$(C_9^{NP}, C_{10}')$
[0.10, 0.98]	$0.979 \pm 0.005$	$0.910 \pm 0.025$	$0.893 \pm 0.015$	$0.882 \pm 0.022$	$0.839 \pm 0.044$	$0.890 \pm 0.027$	$0.857 \pm 0.040$	$0.846 \pm 0.040$
[1.1, 2.5]	$0.994 \pm 0.005$	$0.854 \pm 0.022$	$0.826 \pm 0.010$	$0.803 \pm 0.012$	$0.735 \pm 0.037$	$0.815 \pm 0.019$	$0.761 \pm 0.035$	$0.737 \pm 0.030$
[2.5, 4.0]	$0.995 \pm 0.005$	$0.829 \pm 0.014$	$0.810 \pm 0.012$	$0.779 \pm 0.006$	$0.713 \pm 0.028$	$0.788 \pm 0.010$	$0.734 \pm 0.024$	$0.707 \pm 0.019$
[4.0, 6.0]	$0.996 \pm 0.003$	$0.816 \pm 0.009$	$0.810 \pm 0.011$	$0.773 \pm 0.005$	$0.708 \pm 0.025$	$0.776 \pm 0.005$	$0.723 \pm 0.019$	$0.697 \pm 0.015$
[1.1, 6.0]	$0.995 \pm 0.002$	$0.831 \pm 0.014$	$0.814 \pm 0.010$	$0.783 \pm 0.005$	$0.717 \pm 0.028$	$0.790 \pm 0.010$	$0.737 \pm 0.024$	$0.711 \pm 0.020$
[0.045, 6.0]	$0.976 \pm 0.005$	$0.842 \pm 0.016$	$0.827 \pm 0.007$	$0.802 \pm 0.010$	$0.744 \pm 0.033$	$0.809 \pm 0.015$	$0.762 \pm 0.029$	$0.742 \pm 0.026$

TABLE XVI: The binned average central values and the corresponding  $1\sigma$  uncertainties for the ratio of branching ratio  $\langle R_{f_2'} \rangle$  of  $B_s \rightarrow f_2'(1525)(\rightarrow K^+ K^-) \mu^+ \mu^-$  decays in the SM and in several NP cases.

$q^2$ bins (GeV <sup>2</sup> )	$\langle Q_1 \rangle$							
	SM	$C_9^{NP}$	$C_{10}^{NP}$	$C_9^{NP} = -C_{10}^{NP}$	$C_9^{NP} = -C_9'$	$(C_9^{NP}, C_{10}^{NP})$	$(C_9^{NP}, C_9')$	$(C_9^{NP}, C_{10}')$
[0.10, 0.98]	$0.000 \pm 0.003$	$-0.002 \pm 0.008$	$0.001 \pm 0.008$	$-0.000 \pm 0.001$	$-0.069 \pm 0.016$	$-0.002 \pm 0.005$	$-0.043 \pm 0.013$	$0.004 \pm 0.011$
[1.1, 2.5]	$-0.000 \pm 0.001$	$0.002 \pm 0.028$	$0.010 \pm 0.051$	$0.007 \pm 0.045$	$-0.181 \pm 0.032$	$0.004 \pm 0.036$	$-0.113 \pm 0.032$	$0.095 \pm 0.046$
[2.5, 4.0]	$-0.000 \pm 0.000$	$0.009 \pm 0.060$	$0.003 \pm 0.017$	$0.007 \pm 0.039$	$-0.055 \pm 0.079$	$0.010 \pm 0.059$	$-0.037 \pm 0.075$	$0.181 \pm 0.076$
[4.0, 6.0]	$-0.000 \pm 0.000$	$0.006 \pm 0.035$	$-0.002 \pm 0.019$	$0.002 \pm 0.009$	$0.069 \pm 0.054$	$0.005 \pm 0.028$	$0.039 \pm 0.047$	$0.183 \pm 0.046$
[1.1, 6.0]	$-0.001 \pm 0.002$	$0.010 \pm 0.048$	$0.003 \pm 0.014$	$0.008 \pm 0.035$	$-0.021 \pm 0.066$	$0.011 \pm 0.049$	$-0.014 \pm 0.062$	$0.163 \pm 0.062$
[0.045, 6.0]	$-0.014 \pm 0.040$	$-0.007 \pm 0.009$	$-0.005 \pm 0.016$	$-0.004 \pm 0.006$	$-0.046 \pm 0.032$	$-0.005 \pm 0.003$	$-0.034 \pm 0.019$	$0.084 \pm 0.021$

TABLE XVII: The binned average central values and the corresponding  $1\sigma$  uncertainties for  $\langle Q_1 \rangle$  of  $B_s \rightarrow f_2'(1525)(\rightarrow K^+ K^-) \mu^+ \mu^-$  decays in the SM and in several NP cases.

$q^2$ bins (GeV <sup>2</sup> )	$\langle Q_2 \rangle$							
	SM	$C_9^{NP}$	$C_{10}^{NP}$	$C_9^{NP} = -C_{10}^{NP}$	$C_9^{NP} = -C_9'$	$(C_9^{NP}, C_{10}^{NP})$	$(C_9^{NP}, C_9')$	$(C_9^{NP}, C_{10}')$
[0.10, 0.98]	$0.026 \pm 0.005$	$0.023 \pm 0.004$	$0.001 \pm 0.001$	$0.008 \pm 0.002$	$0.022 \pm 0.005$	$0.016 \pm 0.003$	$0.022 \pm 0.004$	$0.022 \pm 0.005$
[1.1, 2.5]	$0.005 \pm 0.002$	$0.056 \pm 0.049$	$0.010 \pm 0.019$	$0.036 \pm 0.038$	$0.043 \pm 0.052$	$0.051 \pm 0.049$	$0.055 \pm 0.057$	$0.063 \pm 0.060$
[2.5, 4.0]	$-0.001 \pm 0.001$	$0.193 \pm 0.025$	$-0.008 \pm 0.025$	$0.098 \pm 0.018$	$0.194 \pm 0.030$	$0.175 \pm 0.021$	$0.225 \pm 0.033$	$0.243 \pm 0.036$
[4.0, 6.0]	$-0.001 \pm 0.001$	$0.160 \pm 0.030$	$-0.037 \pm 0.007$	$0.048 \pm 0.021$	$0.172 \pm 0.031$	$0.130 \pm 0.030$	$0.198 \pm 0.034$	$0.210 \pm 0.040$
[1.1, 6.0]	$-0.003 \pm 0.001$	$0.167 \pm 0.017$	$-0.014 \pm 0.013$	$0.076 \pm 0.012$	$0.171 \pm 0.020$	$0.147 \pm 0.015$	$0.198 \pm 0.022$	$0.213 \pm 0.027$
[0.045, 6.0]	$-0.007 \pm 0.019$	$0.095 \pm 0.005$	$-0.009 \pm 0.017$	$0.041 \pm 0.008$	$0.096 \pm 0.007$	$0.082 \pm 0.004$	$0.112 \pm 0.010$	$0.121 \pm 0.014$

TABLE XVIII: The binned average central values and the corresponding  $1\sigma$  uncertainties for  $\langle Q_2 \rangle$  of  $B_s \rightarrow f_2'(1525)(\rightarrow K^+ K^-) \mu^+ \mu^-$  decays in the SM and in several NP cases.

$q^2$ bins (GeV <sup>2</sup> )	$\langle Q_4' \rangle$							
	SM	$C_9^{NP}$	$C_{10}^{NP}$	$C_9^{NP} = -C_{10}^{NP}$	$C_9^{NP} = -C_9'$	$(C_9^{NP}, C_{10}^{NP})$	$(C_9^{NP}, C_9')$	$(C_9^{NP}, C_{10}')$
[0.10, 0.98]	$0.011 \pm 0.005$	$0.116 \pm 0.022$	$-0.084 \pm 0.012$	$-0.007 \pm 0.005$	$0.268 \pm 0.052$	$0.073 \pm 0.016$	$0.228 \pm 0.045$	$0.096 \pm 0.026$
[1.1, 2.5]	$0.002 \pm 0.001$	$0.007 \pm 0.050$	$-0.159 \pm 0.029$	$-0.109 \pm 0.017$	$0.102 \pm 0.090$	$-0.042 \pm 0.041$	$0.070 \pm 0.082$	$-0.082 \pm 0.068$
[2.5, 4.0]	$0.000 \pm 0.000$	$-0.050 \pm 0.024$	$-0.058 \pm 0.039$	$-0.073 \pm 0.025$	$-0.049 \pm 0.045$	$-0.068 \pm 0.021$	$-0.054 \pm 0.039$	$-0.167 \pm 0.028$
[4.0, 6.0]	$0.000 \pm 0.000$	$-0.027 \pm 0.014$	$-0.012 \pm 0.017$	$-0.025 \pm 0.014$	$-0.077 \pm 0.016$	$-0.031 \pm 0.014$	$-0.060 \pm 0.014$	$-0.128 \pm 0.021$
[1.1, 6.0]	$0.004 \pm 0.001$	$-0.033 \pm 0.020$	$-0.067 \pm 0.032$	$-0.069 \pm 0.019$	$-0.028 \pm 0.044$	$-0.054 \pm 0.016$	$-0.032 \pm 0.037$	$-0.138 \pm 0.023$
[0.045, 6.0]	$0.098 \pm 0.015$	$0.088 \pm 0.016$	$-0.010 \pm 0.027$	$0.013 \pm 0.010$	$0.132 \pm 0.047$	$0.054 \pm 0.010$	$0.117 \pm 0.039$	$0.008 \pm 0.023$

TABLE XIX: The binned average central values and the corresponding  $1\sigma$  uncertainties for  $\langle Q_4' \rangle$  of  $B_s \rightarrow f_2'(1525)(\rightarrow K^+ K^-) \mu^+ \mu^-$  decays in the SM and in several NP cases.

$q^2$ bins (GeV <sup>2</sup> )	$\langle Q_5' \rangle$							
	SM	$C_9^{NP}$	$C_{10}^{NP}$	$C_9^{NP} = -C_{10}^{NP}$	$C_9^{NP} = -C_9'$	$(C_9^{NP}, C_{10}^{NP})$	$(C_9^{NP}, C_9')$	$(C_9^{NP}, C_{10}')$
[0.10, 0.98]	$0.039 \pm 0.011$	$0.155 \pm 0.016$	$-0.009 \pm 0.004$	$0.066 \pm 0.007$	$0.232 \pm 0.033$	$0.129 \pm 0.013$	$0.223 \pm 0.027$	$0.145 \pm 0.014$
[1.1, 2.5]	$-0.002 \pm 0.004$	$0.248 \pm 0.040$	$-0.009 \pm 0.012$	$0.115 \pm 0.016$	$0.276 \pm 0.031$	$0.217 \pm 0.033$	$0.309 \pm 0.041$	$0.240 \pm 0.042$
[2.5, 4.0]	$-0.004 \pm 0.002$	$0.261 \pm 0.043$	$-0.054 \pm 0.021$	$0.082 \pm 0.029$	$0.249 \pm 0.052$	$0.212 \pm 0.040$	$0.306 \pm 0.054$	$0.258 \pm 0.052$
[4.0, 6.0]	$-0.004 \pm 0.001$	$0.179 \pm 0.041$	$-0.049 \pm 0.016$	$0.031 \pm 0.018$	$0.139 \pm 0.055$	$0.132 \pm 0.036$	$0.195 \pm 0.056$	$0.163 \pm 0.054$
[1.1, 6.0]	$-0.007 \pm 0.002$	$0.229 \pm 0.035$	$-0.035 \pm 0.014$	$0.076 \pm 0.023$	$0.217 \pm 0.044$	$0.187 \pm 0.032$	$0.269 \pm 0.045$	$0.224 \pm 0.043$
[0.045, 6.0]	$-0.071 \pm 0.021$	$0.131 \pm 0.015$	$-0.070 \pm 0.020$	$0.019 \pm 0.018$	$0.139 \pm 0.029$	$0.103 \pm 0.016$	$0.175 \pm 0.023$	$0.126 \pm 0.017$

TABLE XX: The binned average central values and the corresponding  $1\sigma$  uncertainties for  $\langle Q_5' \rangle$  of  $B_s \rightarrow f_2'(1525)(\rightarrow K^+ K^-) \mu^+ \mu^-$  decays in the SM and in several NP cases.

$q^2$ bins (GeV <sup>2</sup> )	$\langle Q_{AFB} \rangle$							
	SM	$C_9^{NP}$	$C_{10}^{NP}$	$C_9^{NP} = -C_{10}^{NP}$	$C_9^{NP} = -C_9'$	$(C_9^{NP}, C_{10}^{NP})$	$(C_9^{NP}, C_9')$	$(C_9^{NP}, C_{10}')$
[0.10, 0.98]	$-0.010 \pm 0.002$	$0.001 \pm 0.003$	$-0.018 \pm 0.004$	$-0.009 \pm 0.004$	$0.010 \pm 0.005$	$-0.002 \pm 0.004$	$0.008 \pm 0.005$	$0.010 \pm 0.005$
[1.1, 2.5]	$-0.002 \pm 0.001$	$0.043 \pm 0.010$	$-0.002 \pm 0.001$	$0.021 \pm 0.006$	$0.064 \pm 0.013$	$0.039 \pm 0.010$	$0.064 \pm 0.014$	$0.072 \pm 0.017$
[2.5, 4.0]	$0.000 \pm 0.001$	$0.055 \pm 0.015$	$-0.000 \pm 0.001$	$0.025 \pm 0.007$	$0.063 \pm 0.017$	$0.048 \pm 0.013$	$0.072 \pm 0.019$	$0.079 \pm 0.022$
[4.0, 6.0]	$0.001 \pm 0.000$	$0.054 \pm 0.014$	$-0.002 \pm 0.002$	$0.020 \pm 0.005$	$0.048 \pm 0.017$	$0.044 \pm 0.012$	$0.062 \pm 0.018$	$0.068 \pm 0.021$
[1.1, 6.0]	$-0.000 \pm 0.001$	$0.052 \pm 0.013$	$-0.001 \pm 0.001$	$0.023 \pm 0.006$	$0.058 \pm 0.016$	$0.045 \pm 0.012$	$0.067 \pm 0.017$	$0.074 \pm 0.020$
[0.045, 6.0]	$-0.004 \pm 0.001$	$0.038 \pm 0.008$	$-0.004 \pm 0.001$	$0.015 \pm 0.003$	$0.045 \pm 0.009$	$0.032 \pm 0.007$	$0.050 \pm 0.010$	$0.056 \pm 0.012$

TABLE XXI: The binned average central values and the corresponding  $1\sigma$  uncertainties for  $\langle Q_{AFB} \rangle$  of  $B_s \rightarrow f_2'(1525)(\rightarrow K^+ K^-) \mu^+ \mu^-$  decays in the SM and in several NP cases.

$q^2$ bins (GeV <sup>2</sup> )	$\langle Q_{FL} \rangle$							
	SM	$C_9^{NP}$	$C_{10}^{NP}$	$C_9^{NP} = -C_{10}^{NP}$	$C_9^{NP} = -C_9'$	$(C_9^{NP}, C_{10}^{NP})$	$(C_9^{NP}, C_9')$	$(C_9^{NP}, C_{10}')$
[0.10, 0.98]	$0.001 \pm 0.001$	$-0.066 \pm 0.005$	$-0.040 \pm 0.004$	$-0.063 \pm 0.004$	$-0.116 \pm 0.011$	$-0.073 \pm 0.005$	$-0.107 \pm 0.010$	$-0.117 \pm 0.009$
[1.1, 2.5]	$0.002 \pm 0.001$	$-0.054 \pm 0.015$	$0.003 \pm 0.009$	$-0.026 \pm 0.013$	$-0.095 \pm 0.023$	$-0.049 \pm 0.015$	$-0.089 \pm 0.022$	$-0.096 \pm 0.025$
[2.5, 4.0]	$0.002 \pm 0.001$	$-0.030 \pm 0.010$	$0.020 \pm 0.005$	$-0.001 \pm 0.006$	$-0.072 \pm 0.018$	$-0.021 \pm 0.010$	$-0.061 \pm 0.016$	$-0.064 \pm 0.019$
[4.0, 6.0]	$0.002 \pm 0.000$	$-0.016 \pm 0.006$	$0.020 \pm 0.003$	$0.007 \pm 0.002$	$-0.062 \pm 0.016$	$-0.008 \pm 0.005$	$-0.046 \pm 0.011$	$-0.047 \pm 0.014$
[1.1, 6.0]	$0.002 \pm 0.001$	$-0.030 \pm 0.010$	$0.015 \pm 0.004$	$-0.005 \pm 0.007$	$-0.075 \pm 0.017$	$-0.023 \pm 0.010$	$-0.063 \pm 0.015$	$-0.066 \pm 0.018$
[0.045, 6.0]	$0.012 \pm 0.002$	$-0.038 \pm 0.007$	$-0.001 \pm 0.006$	$-0.023 \pm 0.008$	$-0.089 \pm 0.012$	$-0.038 \pm 0.009$	$-0.078 \pm 0.011$	$-0.085 \pm 0.014$

TABLE XXII: The binned average central values and the corresponding  $1\sigma$  uncertainties for  $\langle Q_{FL} \rangle$  of  $B_s \rightarrow f_2'(1525)(\rightarrow K^+ K^-) \mu^+ \mu^-$  decays in the SM and in several NP cases.

- 
- [1] R. Aaij *et al.* [LHCb], “Search for lepton-universality violation in  $B^+ \rightarrow K^+\ell^+\ell^-$  decays,” *Phys. Rev. Lett.* **122**, no.19, 191801 (2019) doi:10.1103/PhysRevLett.122.191801 [arXiv:1903.09252 [hep-ex]].
- [2] G. Hiller and F. Kruger, “More model-independent analysis of  $b \rightarrow s$  processes,” *Phys. Rev. D* **69**, 074020 (2004) doi:10.1103/PhysRevD.69.074020 [arXiv:hep-ph/0310219 [hep-ph]].
- [3] M. Bordone, G. Isidori and A. Pattori, “On the Standard Model predictions for  $R_K$  and  $R_{K^*}$ ,” *Eur. Phys. J. C* **76**, no.8, 440 (2016) doi:10.1140/epjc/s10052-016-4274-7 [arXiv:1605.07633 [hep-ph]].
- [4] R. Aaij *et al.* [LHCb], “Test of lepton universality with  $B^0 \rightarrow K^{*0}\ell^+\ell^-$  decays,” *JHEP* **08**, 055 (2017) doi:10.1007/JHEP08(2017)055 [arXiv:1705.05802 [hep-ex]].
- [5] A. Abdesselam *et al.* [Belle], “Test of lepton flavor universality in  $B \rightarrow K^*\ell^+\ell^-$  decays at Belle,” [arXiv:1904.02440 [hep-ex]].
- [6] S. Descotes-Genon, J. Matias, M. Ramon and J. Virto, “Implications from clean observables for the binned analysis of  $B^- \rightarrow K^-\mu^+\mu^-$  at large recoil,” *JHEP* **01**, 048 (2013) doi:10.1007/JHEP01(2013)048 [arXiv:1207.2753 [hep-ph]].
- [7] S. Descotes-Genon, T. Hurth, J. Matias and J. Virto, “Optimizing the basis of  $B \rightarrow K^*\ell\ell$  observables in the full kinematic range,” *JHEP* **05**, 137 (2013) doi:10.1007/JHEP05(2013)137 [arXiv:1303.5794 [hep-ph]].
- [8] M. Aaboud *et al.* [ATLAS], “Angular analysis of  $B_d^0 \rightarrow K^{*0}\mu^+\mu^-$  decays in  $pp$  collisions at  $\sqrt{s} = 8$  TeV with the ATLAS detector,” *JHEP* **10**, 047 (2018) doi:10.1007/JHEP10(2018)047 [arXiv:1805.04000 [hep-ex]].
- [9] R. Aaij *et al.* [LHCb], “Measurement of Form-Factor-Independent Observables in the Decay  $B^0 \rightarrow K^{*0}\mu^+\mu^-$ ,” *Phys. Rev. Lett.* **111**, 191801 (2013) doi:10.1103/PhysRevLett.111.191801 [arXiv:1308.1707 [hep-ex]].
- [10] R. Aaij *et al.* [LHCb], “Angular analysis of the  $B^0 \rightarrow K^{*0}\mu^+\mu^-$  decay using  $3 \text{ fb}^{-1}$  of integrated luminosity,” *JHEP* **02**, 104 (2016) doi:10.1007/JHEP02(2016)104 [arXiv:1512.04442 [hep-ex]].
- [11] J. Aebischer, J. Kumar, P. Stangl and D. M. Straub, “A Global Likelihood for Precision Constraints and Flavour Anomalies,” *Eur. Phys. J. C* **79**, no.6, 509 (2019) doi:10.1140/epjc/s10052-019-6977-z [arXiv:1810.07698 [hep-ph]].
- [12] CMS Collaboration, “Measurement of the  $P_1$  and  $P'_5$  angular parameters of the decay  $B^0 \rightarrow K^{*0}\mu^+\mu^-$  in proton-proton collisions at  $\sqrt{s} = 8$  TeV” [CMS-PAS-BPH-15-008].
- [13] A. Abdesselam *et al.* [Belle], “Angular analysis of  $B^0 \rightarrow K^*(892)^0\ell^+\ell^-$ ,” [arXiv:1604.04042 [hep-ex]].
- [14] S. Descotes-Genon, L. Hofer, J. Matias and J. Virto, *JHEP* **12**, 125 (2014) doi:10.1007/JHEP12(2014)125 [arXiv:1407.8526 [hep-ph]].
- [15] R. Aaij *et al.* [LHCb], “Differential branching fraction and angular analysis of the decay  $B_s^0 \rightarrow \phi\mu^+\mu^-$ ,” *JHEP* **07**, 084 (2013) doi:10.1007/JHEP07(2013)084 [arXiv:1305.2168 [hep-ex]].
- [16] R. Aaij *et al.* [LHCb], “Angular analysis and differential branching fraction of the decay  $B_s^0 \rightarrow \phi\mu^+\mu^-$ ,” *JHEP* **09**, 179 (2015) doi:10.1007/JHEP09(2015)179 [arXiv:1506.08777 [hep-ex]].
- [17] A. Bharucha, D. M. Straub and R. Zwicky, “ $B \rightarrow V\ell^+\ell^-$  in the Standard Model from light-cone sum rules,” *JHEP* **08**, 098 (2016) doi:10.1007/JHEP08(2016)098 [arXiv:1503.05534 [hep-ph]].
- [18] R. H. Li, C. D. Lu and W. Wang, “Branching ratios, forward-backward asymmetries and angular distributions of  $B \rightarrow K_2^*l^+l^-$  in the standard model and new physics scenarios,” *Phys. Rev. D* **83**, 034034 (2011) doi:10.1103/PhysRevD.83.034034 [arXiv:1012.2129 [hep-ph]].
- [19] I. Ahmed, M. J. Aslam, M. Junaid and S. Shafaq, “Model independent analysis of  $B \rightarrow \ell K^*(2)(1430)\mu^+\mu^-$  decay,” *JHEP* **02**, 045 (2012) doi:10.1007/JHEP02(2012)045
- [20] S. Rai Choudhury, A. S. Cornell, G. C. Joshi and B. H. J. McKellar, “Analysis of the  $B \rightarrow \ell K^*(2)(\rightarrow \ell K \pi) l^+ l^-$  decay,” *Phys. Rev. D* **74**, 054031 (2006) doi:10.1103/PhysRevD.74.054031 [arXiv:hep-ph/0607289 [hep-ph]].
- [21] H. Hatanaka and K. C. Yang, “Radiative and Semileptonic B Decays Involving the Tensor Meson  $K(2)^*(1430)$  in the Standard Model and Beyond,” *Phys. Rev. D* **79**, 114008 (2009) doi:10.1103/PhysRevD.79.114008 [arXiv:0903.1917 [hep-ph]].
- [22] H. Hatanaka and K. C. Yang, “Radiative and Semileptonic B Decays Involving Higher K-Resonances in the Final States,” *Eur. Phys. J. C* **67**, 149-162 (2010) doi:10.1140/epjc/s10052-010-1293-7 [arXiv:0907.1496 [hep-ph]].
- [23] M. Junaid, M. J. Aslam and I. Ahmed, “Complementarity of Semileptonic  $B$  to  $K_2^*(1430)$  and  $K^*(892)$  Decays in the Standard Model with Fourth Generation,” *Int. J. Mod. Phys. A* **27**, 1250149 (2012) doi:10.1142/S0217751X12501497 [arXiv:1103.3934 [hep-ph]].
- [24] C. D. Lu and W. Wang, “Analysis of  $B \rightarrow K_J^*(\rightarrow K\pi)\mu^+\mu^-$  in the higher kaon resonance region,” *Phys. Rev. D* **85**, 034014 (2012) doi:10.1103/PhysRevD.85.034014 [arXiv:1111.1513 [hep-ph]].
- [25] T. M. Aliev and M. Savci, “ $B \rightarrow K_2\ell^+\ell^-$  decay beyond the Standard Model,” *Phys. Rev. D* **85**, 015007 (2012) doi:10.1103/PhysRevD.85.015007 [arXiv:1109.2738 [hep-ph]].
- [26] D. Das, B. Kindra, G. Kumar and N. Mahajan, “ $B \rightarrow K_2^*(1430)\ell^+\ell^-$  distributions at large recoil in the Standard Model and beyond,” *Phys. Rev. D* **99**, no.9, 093012 (2019) doi:10.1103/PhysRevD.99.093012 [arXiv:1812.11803 [hep-ph]].
- [27] R. Dutta, “Model independent analysis of new physics effects on  $B_c \rightarrow (D_s, D_s^*)\mu^+\mu^-$  decay observables,” *Phys. Rev. D* **100**, no.7, 075025 (2019) doi:10.1103/PhysRevD.100.075025 [arXiv:1906.02412 [hep-ph]].
- [28] A. J. Buras and M. Munz, “Effective Hamiltonian for  $B \rightarrow \ell X(s) e^+ e^-$  beyond leading logarithms in the NDR and HV schemes,” *Phys. Rev. D* **52**, 186-195 (1995) doi:10.1103/PhysRevD.52.186 [arXiv:hep-ph/9501281 [hep-ph]].
- [29] A. K. Alok, A. Datta, A. Dighe, M. Duraisamy, D. Ghosh and D. London, “New Physics in  $b \rightarrow s\mu^+\mu^-$ : CP-Conserving Observables,” *JHEP* **11**, 121 (2011) doi:10.1007/JHEP11(2011)121 [arXiv:1008.2367 [hep-ph]].
- [30] A. K. Alok, A. Datta, A. Dighe, M. Duraisamy, D. Ghosh and D. London, “New Physics in  $b \rightarrow \ell s \mu^+ \mu^-$ : CP-Violating

- Observables,” JHEP **11**, 122 (2011) doi:10.1007/JHEP11(2011)122 [arXiv:1103.5344 [hep-ph]].
- [31] D. Bardhan, P. Byakti and D. Ghosh, “Role of Tensor operators in  $R_K$  and  $R_{K^*}$ ,” Phys. Lett. B **773**, 505-512 (2017) doi:10.1016/j.physletb.2017.08.062 [arXiv:1705.09305 [hep-ph]].
- [32] A. K. Alok, A. Dighe, S. Gangal and D. Kumar, “Continuing search for new physics in  $b \rightarrow s\mu\mu$  decays: two operators at a time,” JHEP **06**, 089 (2019) doi:10.1007/JHEP06(2019)089 [arXiv:1903.09617 [hep-ph]].
- [33] E. R. Berger, A. Donnachie, H. G. Dosch and O. Nachtmann, “Observing the odderon: Tensor meson photoproduction,” Eur. Phys. J. C **14**, 673-682 (2000) doi:10.1007/s100520000377 [arXiv:hep-ph/0001270 [hep-ph]].
- [34] W. Wang, “B to tensor meson form factors in the perturbative QCD approach,” Phys. Rev. D **83**, 014008 (2011) doi:10.1103/PhysRevD.83.014008 [arXiv:1008.5326 [hep-ph]].
- [35] K. C. Yang, “B to Light Tensor Meson Form Factors Derived from Light-Cone Sum Rules,” Phys. Lett. B **695**, 444-448 (2011) doi:10.1016/j.physletb.2010.11.053 [arXiv:1010.2944 [hep-ph]].
- [36] B. Capdevila, S. Descotes-Genon, J. Matias and J. Virto, “Assessing lepton-flavour non-universality from  $B \rightarrow K^*\ell\ell$  angular analyses,” JHEP **10**, 075 (2016) doi:10.1007/JHEP10(2016)075 [arXiv:1605.03156 [hep-ph]].
- [37] M. Tanabashi *et al.* [Particle Data Group], “Review of Particle Physics,” Phys. Rev. D **98**, no.3, 030001 (2018) doi:10.1103/PhysRevD.98.030001
- [38] A. Ali, P. Ball, L. T. Handoko and G. Hiller, “A Comparative study of the decays  $B \rightarrow (K, K^*)\ell^+\ell^-$  in standard model and supersymmetric theories,” Phys. Rev. D **61**, 074024 (2000) doi:10.1103/PhysRevD.61.074024 [arXiv:hep-ph/9910221 [hep-ph]].
- [39] B. Capdevila, A. Crivellin, S. Descotes-Genon, J. Matias and J. Virto, “Patterns of New Physics in  $b \rightarrow s\ell^+\ell^-$  transitions in the light of recent data,” JHEP **01**, 093 (2018) doi:10.1007/JHEP01(2018)093 [arXiv:1704.05340 [hep-ph]].
- [40] W. Altmannshofer, P. Stangl and D. M. Straub, “Interpreting Hints for Lepton Flavor Universality Violation,” Phys. Rev. D **96**, no.5, 055008 (2017) doi:10.1103/PhysRevD.96.055008 [arXiv:1704.05435 [hep-ph]].
- [41] G. D’Amico, M. Nardecchia, P. Panci, F. Sannino, A. Strumia, R. Torre and A. Urbano, “Flavour anomalies after the  $R_{K^*}$  measurement,” JHEP **09**, 010 (2017) doi:10.1007/JHEP09(2017)010 [arXiv:1704.05438 [hep-ph]].
- [42] G. Hiller and I. Nisandzic, “ $R_K$  and  $R_{K^*}$  beyond the standard model,” Phys. Rev. D **96**, no.3, 035003 (2017) doi:10.1103/PhysRevD.96.035003 [arXiv:1704.05444 [hep-ph]].
- [43] L. S. Geng, B. Grinstein, S. Jger, J. Martin Camalich, X. L. Ren and R. X. Shi, “Towards the discovery of new physics with lepton-universality ratios of  $b \rightarrow s\ell\ell$  decays,” Phys. Rev. D **96**, no.9, 093006 (2017) doi:10.1103/PhysRevD.96.093006 [arXiv:1704.05446 [hep-ph]].
- [44] M. Ciuchini, A. M. Coutinho, M. Fedele, E. Franco, A. Paul, L. Silvestrini and M. Valli, “On Flavourful Easter eggs for New Physics hunger and Lepton Flavour Universality violation,” Eur. Phys. J. C **77**, no.10, 688 (2017) doi:10.1140/epjc/s10052-017-5270-2 [arXiv:1704.05447 [hep-ph]].
- [45] A. Celis, J. Fuentes-Martin, A. Vicente and J. Virto, “Gauge-invariant implications of the LHCb measurements on lepton-flavor nonuniversality,” Phys. Rev. D **96**, no.3, 035026 (2017) doi:10.1103/PhysRevD.96.035026 [arXiv:1704.05672 [hep-ph]].
- [46] A. K. Alok, B. Bhattacharya, A. Datta, D. Kumar, J. Kumar and D. London, “New Physics in  $b \rightarrow s\mu^+\mu^-$  after the Measurement of  $R_{K^*}$ ,” Phys. Rev. D **96**, no.9, 095009 (2017) doi:10.1103/PhysRevD.96.095009 [arXiv:1704.07397 [hep-ph]].
- [47] A. K. Alok, B. Bhattacharya, D. Kumar, J. Kumar, D. London and S. U. Sankar, “New physics in  $b \rightarrow s\mu^+\mu^-$ : Distinguishing models through CP-violating effects,” Phys. Rev. D **96**, no.1, 015034 (2017) doi:10.1103/PhysRevD.96.015034 [arXiv:1703.09247 [hep-ph]].